SMRA 2022

Clinical Benefits of MR Angiography

Recent Innovations in Non-Contrast MRA

Robert R. Edelman, Ioannis Koktzoglou
Northshore University HealthSystem, Evanston, IL, USA

3D Whole Heart Applications: Angiography and Delayed Enhancement

Jason Craft, et al.
St Francis Heart Hospital, DeMatteis Research Center, Greenvale, NY, USA

Infrared Thermally Enhanced 3D TOF MOTSA MRA for Visualizing the Arteries of the Face

Marc Mespreuve, et al.
University Hospital Ghent; AZ St Maarten, Mechelen, Belgium

Magnetic Resonance Angiography with Ferumoxytol

J. Paul Finn, Kim-Lien Nguyen, et al.
David Geffen School of Medicine at UCLA, Los Angeles, CA, USA

High Spatial Resolution Coronary MRA

Reza Hajhosseiny, René M. Botnar, et al.
School of Biomedical Engineering and Imaging Sciences, King's College London, United Kingdom

SIEMENS Healthineers

Recent Innovations in Non-Contrast MR Angiography: The NorthShore Experience

Robert R. Edelman, M.D.[1,2]; Ioannis Koktzoglou, Ph.D.[1,3]

[1]Radiology, Northshore University HealthSystem, Evanston, IL, USA
[2]Radiology, Feinberg School of Medicine, Northwestern University, Chicago, IL, USA
[3]Radiology, Pritzker School of Medicine, University of Chicago, Chicago, IL, USA

CT angiography (CTA) and contrast-enhanced MR angiography (CEMRA) are routinely used as noninvasive alternatives to digital subtraction angiography for the evaluation of suspected vascular disorders and for pre-surgical mapping of vascular anatomy [1–3]. For patients with impaired renal function, poor venous access, or contrast allergy, non-contrast MRA can provide a useful alternative to these contrast-enhanced imaging modalities. Several non-contrast MRA techniques are commercially available, including time-of-flight MRA for the evaluation of the neurovascular system [4], NATIVE TrueFISP for the evaluation of the renal and mesenteric arteries [5, 6], and quiescent interval single-shot (QISS) for the evaluation of the lower-extremity peripheral arteries [7, 8]. While these techniques have proven accurate and are straightforward to use, recent innovations promise further improvements. In this article, we will present examples of new non-contrast MRA techniques under development by our research group which aim to shorten scan time, improve reliability, add functional information, and expand the breadth of clinical applications. These techniques include radial QISS[1] [9, 10], stack-of-stars fast interrupted steady-state (FISS)[1] [11], dark blood imaging using 3D unbalanced steady-state free precession (3D uSSFP)[1] [12], and quantitative time-of-flight (qTOF)[1] [13].

Radial QISS

Standard contrast-enhanced and non-contrast MRA techniques, including the commercially available versions of QISS, typically use a Cartesian *k*-space trajectory. Cartesian *k*-space trajectories have historically been preferred because they tended to provide more consistent image quality than non-Cartesian techniques, with fewer artifacts from static magnetic field inhomogeneity and gradient-induced eddy currents. However, a drawback of Cartesian *k*-space trajectories with respect to motion artifact is that the center of *k*-space has a dominant impact on image contrast. As a result, any patient motion or other cause of inconsistent signal intensity during the acquisition of the central *k*-space lines (including respiration, highly pulsatile blood flow, or cardiac arrythmias) will result in image artifacts that manifest as repetitive ghost artifacts along the phase-encoding and slab-encoding directions.

However, using state-of-the-art MRI hardware and software, non-Cartesian *k*-space trajectories can provide reliably good image quality. Moreover, radial techniques

1 Patient with atrial fibrillation and irregular cardiac rhythm undergoing non-contrast evaluation of the lower-extremity peripheral arteries. **(1A)** ECG recording during MRI exam shows an irregular heart rhythm. **(1B)** Standard Cartesian QISS shows severe banding artifacts that render the study non-diagnostic. **(1C)** Radial QISS shows few artifacts and provides a diagnostic examination.

[1]*Work in progress. The application is currently under development and is not for sale in the U.S. and in other countries. Its future availability cannot be ensured.*

are known to be less sensitive to patient motion than Cartesian ones [14]. In this regard, we have begun exploring the use of a non-Cartesian radial QISS acquisition for several clinical applications, including imaging of the aorta, pulmonary vessels, and peripheral vasculature [9, 10]. We have found that radial QISS, using comparable spatial resolution and scan time to commercially available Cartesian versions of the technique, is much less sensitive to patient motion. As a result, it permits imaging of the abdominal and pelvic vessels with fewer artifacts during free-breathing or failed breath-holds. Moreover, it is less sensitive to ECG gating artifacts in patients with arrhythmias and can salvage what would have been a non-diagnostic exam using Cartesian QISS (Fig. 1).

FISS

FISS is a new non-contrast MRA technique that represents a modified form of TrueFISP. In distinction to TrueFISP, where rapid repetition of the sequence generates steady-state magnetization that is uninterrupted over the shot duration, with FISS the echo train is deliberately interrupted at frequent intervals and the in-plane steady-state transverse magnetization is periodically stored along the z-axis [11]. With proper selection of the imaging parameters, FISS provides several benefits over TrueFISP for non-contrast MRA, including suppression of fat signal without the need to apply a separate chemical shift-selective radiofrequency pulse and reduced flow artifacts from accelerating or turbulent flow as well as from flow through poorly shimmed regions.

Three-dimensional FISS using a radial stack-of-stars *k*-space trajectory allows breath-hold evaluation of the renal arteries and other abdominal vessels (Fig. 2) [15], while a 5D version permits motion-resolved imaging of the heart without the need for cardiac or respiratory gating [16]. More recently, we have begun testing a single-shot free-breathing navigator-gated version of 3D FISS, which can match or exceed the image quality of native TrueFISP despite a three-fold shorter scan time (Fig. 3).

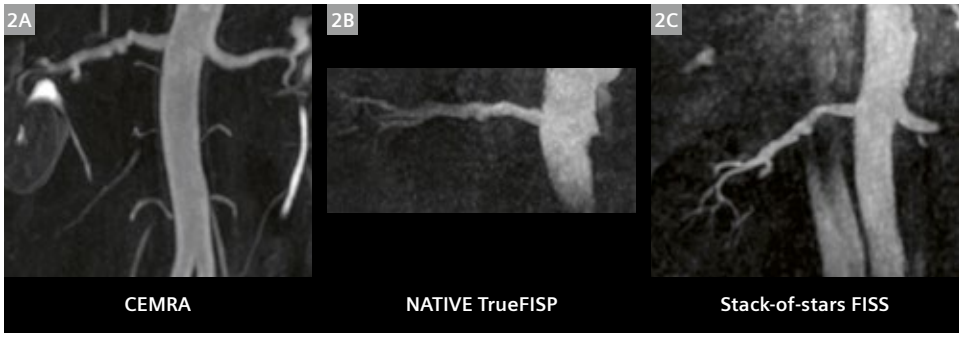

2 56-year-old female with fibromuscular dysplasia of the right renal artery. **(2A)** CEMRA; **(2B)** free-breathing native TrueFISP; **(2C)** breath-hold stack-of-stars FISS. Stack-of-stars FISS demonstrates the irregularities of the right renal artery comparably to the much lengthier native TrueFISP acquisition and better demonstrates the distal portion of the vessel.

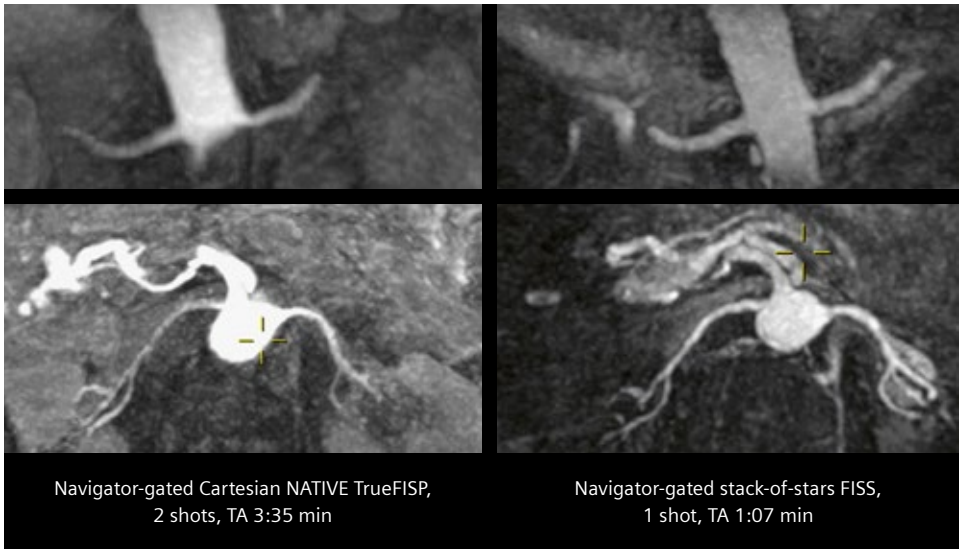

3 71-year-old female with impaired renal function referred for non-contrast renal artery evaluation. Both sequences were acquired using free-breathing and navigator gating. The renal arteries are better shown with stack-of-stars FISS than native TrueFISP despite the 3-fold shorter scan time.

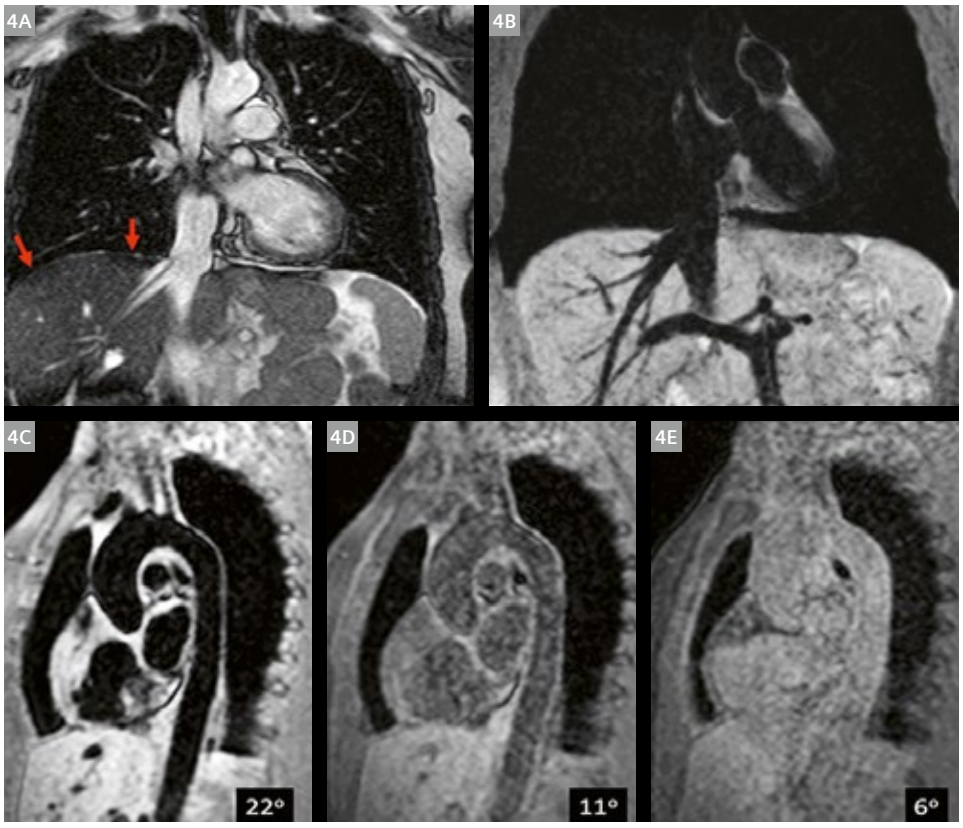

4 Illustration of 3D uSSFP in a healthy volunteer. **(4A)** With TrueFISP, the blood pool appears bright. Off-resonance effects obscure the dome of the right hemidiaphragm (arrows). **(4B)** With 3D uSSFP, the blood pool appears dark. No off-resonance effects are seen. **(4C–E)** With 3D uSSFP, the flip angle has a profound influence on the blood pool signal.

3D uSSFP

While "bright blood" techniques such as CEMRA and TrueFISP are geared towards making the intraluminal blood pool appear bright so as to facilitate the evaluation of luminal patency, it is also possible to directly image abnormalities of the vessel wall such as plaque and dissection using "dark blood" techniques. A 3D turbo spin-echo sequence called *sampling perfection with application-optimized contrasts using different flip angle evolution* (SPACE) has been the preferred technique for dark blood vascular imaging [17]. While useful for dark blood imaging of the intracranial circulation and extracranial carotid arteries, SPACE is inefficient and sensitive to patient motion. We have therefore been exploring the use of an ECG-gated 3D uSSFP sequence which is more efficient and less sensitive to motion [12]. Unlike 3D TrueFISP, which is motion compensated along the slab-encoding and readout directions, 3D uSSFP produces a small amount of flow-related dephasing along both directions with each sequence repetition, resulting in suppression of the intraluminal signal from flowing spins. This sequence has several interesting properties, including the dependence of image contrast and motion sensitivity on the flip angle. For instance, the blood pool will appear gray with a low flip angle but dark with a moderate flip angle on the order of 20 to 30 degrees (Fig. 4). Different from TrueFISP, the technique is insensitive to off-resonance effects. The 3D uSSFP technique may have potential clinical applications for the evaluation of blood vessels in the neck, chest, and abdomen, and we anticipate that it could also prove helpful for the evaluation of pulmonary nodules by improving lesion-to-background contrast.

qTOF

Time-of-flight (TOF) MRA is routinely used to evaluate the neurovascular system. TOF MRA, however, does not provide quantitative hemodynamic information, such as blood flow velocity and volume flow rates. Quantitative time-of-flight (qTOF) is a new method that shows promise for simultaneous hemodynamic and high spatial resolution luminal evaluation of the intracranial arteries without any increase in acquisition time (Fig. 5) [13]. By using a flow-compensated stack-of-stars multi-echo time data acquisition, qTOF portrays the arterial lumen like standard TOF MRA. An automated computer-vision procedure is applied to quantify component (i.e., x, y, z) and total blood flow velocities from small movements of the arterial signal across successively acquired echo times. Volume flow rates

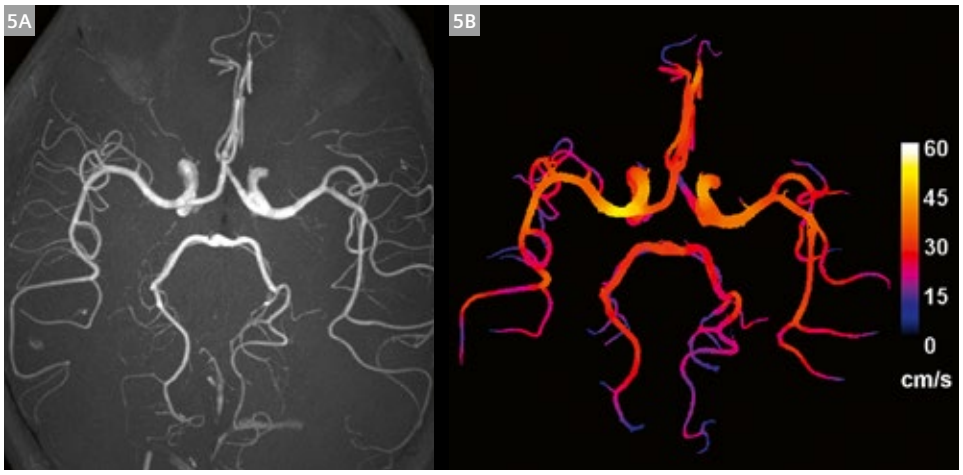

5 Transversal maximum intensity projections showing a high-resolution qTOF MRA of the intracranial arteries **(5A)** and the qTOF-derived mean cross-sectional total flow velocity map **(5B)**. qTOF provides an image appearance that is like standard (non-quantitative) TOF MRA while also providing quantitative hemodynamic information without any increase of the acquisition time.

can be quantified as the product of mean cross-sectional flow velocity and arterial cross-section area, with the latter obtained from the high spatial resolution qTOF MRA. While the main feature of qTOF is the addition of quantitative hemodynamic information at no added cost, the use of stack-of-stars *k*-space sampling with qTOF also eliminates flow-related misregistration artifacts from oblique in-plane blood flow that can distort and obscure luminal anatomy on standard Cartesian TOF MRA.

Conclusion

The technology of non-contrast MRA is advancing at a brisk pace. We expect continual improvements in the speed, accuracy, and reliability of non-contrast MRA, while the breadth of clinical applications will continue to expand.

References

1 Menke J, Larsen J. Meta-analysis: Accuracy of contrast-enhanced magnetic resonance angiography for assessing steno-occlusions in peripheral arterial disease. Ann Intern Med 2010;153(5):325-334.
2 Catalano C, Fraioli F, Laghi A, Napoli A, Bezzi M, Pediconi F, Danti M, Nofroni I, Passariello R. Infrarenal aortic and lower-extremity arterial disease: diagnostic performance of multi-detector row CT angiography. Radiology 2004;231(2):555-563.
3 Willmann JK, Wildermuth S, Pfammatter T, Roos JE, Seifert B, Hilfiker PR, Marincek B, Weishaupt D. Aortoiliac and renal arteries: prospective intraindividual comparison of contrast-enhanced three-dimensional MR angiography and multi-detector row CT angiography. Radiology 2003;226(3):798-811.
4 Alfidi RJ, Masaryk TJ, Haacke EM, Lenz GW, Ross JS, Modic MT, Nelson AD, LiPuma JP, Cohen AM. MR angiography of peripheral, carotid, and coronary arteries.
AJR American journal of roentgenology 1987;149(6):1097-1109.
5 Katoh M, Buecker A, Stuber M, Gunther RW, Spuentrup E. Free-breathing renal MR angiography with steady-state free-precession (SSFP) and slab-selective spin inversion: initial results. Kidney Int 2004;66(3):1272-1278.
6 Wyttenbach R, Braghetti A, Wyss M, Alerci M, Briner L, Santini P, Cozzi L, Di Valentino M, Katoh M, Marone C, Vock P, Gallino A. Renal artery assessment with nonenhanced steady-state free precession versus contrast-enhanced MR angiography. Radiology 2007;245(1):186-195.
7 Amin P, Collins JD, Koktzoglou I, Molvar C, Markl M, Edelman RR, Carr JC. Evaluating peripheral arterial disease with unenhanced quiescent-interval single-shot MR angiography at 3 T. AJR American journal of roentgenology 2014;202(4):886-893.
8 Edelman RR, Sheehan JJ, Dunkle E, Schindler N, Carr J, Koktzoglou I. Quiescent-interval single-shot unenhanced magnetic resonance angiography of peripheral vascular disease: Technical considerations and clinical feasibility. Magn Reson Med 2010;63(4):951-958.
9 Edelman RR, Silvers RI, Thakrar KH, Metzl MD, Nazari J, Giri S, Koktzoglou I. Nonenhanced MR angiography of the pulmonary arteries using single-shot radial quiescent-interval slice-selective (QISS): a technical feasibility study. Journal of cardiovascular magnetic resonance: official journal of the Society for Cardiovascular Magnetic Resonance 2017;19(1):48.
10 Edelman RR, Giri S, Dunkle E, Galizia M, Amin P, Koktzoglou I. Quiescent-inflow single-shot magnetic resonance angiography using a highly undersampled radial k-space trajectory. Magn Reson Med 2013;70(6):1662-1668.
11 Koktzoglou I, Edelman RR. Radial fast interrupted steady-state (FISS) magnetic resonance imaging. Magnetic resonance in medicine 2018;79(4):2077-2086.
12 Edelman RR, Leloudas N, Pang J, Koktzoglou I. Dark blood cardiovascular magnetic resonance of the heart, great vessels, and lungs using electrocardiographic-gated three-dimensional unbalanced steady-state free precession. J Cardiovasc Magn Reson 2021;23(1):127.
13 Koktzoglou I, Huang R, Edelman RR. Quantitative time-of-flight MR angiography for simultaneous luminal and hemodynamic evaluation of the intracranial arteries. Magn Reson Med 2022;87(1):150-162.
14 Glover GH, Pauly JM. Projection reconstruction techniques for reduction of motion effects in MRI. Magnetic resonance in medicine 1992;28(2):275-289.

15 Edelman RR, Pang J, Koktzoglou I. Breath-hold Three-dimensional Quiescent-Interval Slice-Selective (QISS) MR Angiography using a Fast-Interrupted Steady-State (FISS) Readout: Application to the Coronary and Renal Arteries. Proceedings of the 2018 Annual Meeting of the International Society for Magnetic Resonance in Medicine. Paris, France 2018. p 2988.
16 Bastiaansen JAM, Piccini D, Di Sopra L, Roy CW, Heerfordt J, Edelman RR, Koktzoglou I, Yerly J, Stuber M. Natively fat-suppressed 5D whole-heart MRI with a radial free-running fast-interrupted steady-state (FISS) sequence at 1.5T and 3T. Magnetic resonance in medicine 2020;83(1):45-55.
17 Okuchi S, Fushimi Y, Okada T, Yamamoto A, Okada T, Kikuchi T, Yoshida K, Miyamoto S, Togashi K. Visualization of carotid vessel wall and atherosclerotic plaque: T1-SPACE vs. compressed sensing T1-SPACE. Eur Radiol 2019;29(8):4114-4122.

Contact

Robert R. Edelman, M.D.
Walgreen Building, G534
2650 Ridge Avenue
Evanston, IL 60201
USA
redelman@northshore.org

Robert Edelman

Ioannis Koktzoglou

[1]*Törnqvist, E., Månsson, A., Larsson, E.-M., & Hallström, I. (2006). Impact of extended written information on patient anxiety and image motion artifacts during magnetic resonance imaging. Acta Radiologica, 47(5), 474–480. https://doi.org/10.1080/02841850600690355.*

Magnetic Resonance Angiography with Ferumoxytol

J. Paul Finn, M.D.[1,2]; Takegawa Yoshida, M.D.[1]; Ashley Prosper, M.D.[1]; Arash Bedayat, M.D.[1]; Cameron Hassani, M.D.[1]; Puja Shahrouki, M.D.[1]; Kim-Lien Nguyen, M.D.[1,2,3]

[1]Diagnostic Cardiovascular Imaging Section, Department of Radiological Sciences, David Geffen School of Medicine at UCLA, Los Angeles, CA, USA
[2]Physics and Biology in Medicine Graduate Program, University of California, Los Angeles, CA, USA
[3]Division of Cardiology, David Geffen School of Medicine at UCLA and VA Greater Los Angeles Healthcare System, Los Angeles, CA, USA

Introduction

In the more than three decades since magnetic resonance angiography (MRA) was introduced into clinical practice, resolution and imaging speed have improved dramatically. Parallel imaging and advances in coil technology have slashed acquisition times through undersampling, while data processing power has exploded. More recent developments in compressed sensing and deep learning hold promise for still more aggressive undersampling schemes as they usher in an exciting new era of technical innovation. Today, MRA studies are, on average, faster to acquire with greater coverage and higher resolution than 10 years ago, at which time MRA use was growing at a fast pace [1, 2]. However, an analysis of MRA utilization trends over the past decade suggests that its use is steadily decreasing, while the use of X-ray CT angiography (CTA) is steadily increasing [3]. The reasons underlying this trend will require further analysis, but relevant factors in the choice of test include ease of access, diagnostic accuracy, image

1 3-day-old[1] male patient with hypoplastic aortic arch and coarctation. Coronal thin MIP images from ferumoxytol enhanced MRA in the arterial **(1A)**, venous **(1B)** and late venous **(1C)** phases at 3T. Note the stable intravascular signal in the 43-minute interval between the early and late venous phases. *Reproduced from [30] with permission.*

[1]Siemens Healthineers Disclaimer: MR scanning has not been established as safe for imaging fetuses and infants less than two years of age. The responsible physician must evaluate the benefits of the MR examination compared to those of other imaging procedures. Note: This disclaimer does not represent the opinion of the authors.

quality, workflow, cost and safety. Modern CTA has made impressive strides in all of these spaces, raising the bar in a point to point face off [4]. Nonetheless, in certain areas, MRA is still firmly rooted in clinical practice (e.g., 3D Time of Flight MRA in the brain) and is an effective alternative to CTA when iodinated contrast agents are contraindicated or when vascular calcification is problematic. Also, MR technology has unique advantages for imaging the vessel wall and plaque composition [5]. Outside of the brain, contrast enhanced MRA (CEMRA) has out-performed non-contrast techniques for most applications, but the association of gadolinium with nephrogenic systemic fibrosis [6, 7] and gadolinium retention in brain [8, 9] has unwound the common practice of using high dose gadolinium for CEMRA. Although there is strong evidence supporting the safety of the macrocyclic gadolinium-based contrast agents (GBCAs) in patients with renal impairment [10], persistent concerns about gadolinium brain deposition [8, 11] have tempered enthusiasm for GBCA enhanced studies in several patient groups. For all of the above reasons, the landscape of advanced, non-invasive vascular imaging is very much in flux.

Against this background, ferumoxytol (Sandoz Inc, Princeton, NJ, USA: Feraheme®, Covis Pharma GmbH, Zug, Switzerland) has emerged as a diamond in the rough that can address many of the limitations faced by both gadolinium-based MRA and iodine-based CTA [12–17]. Ferumoxytol is an iron nanoparticle with a mean particle diameter of 30 nm [13, 14], placing it in the class of ultrasmall, superparamagnetic iron oxide (USPIO) agents. It is approved in the U.S. for intravenous iron replacement therapy in patients with all levels of renal impairment, as well as in those with normal renal function [18]. Ferumoxytol is effectively a pure blood-pool agent with remarkable MRI properties that has proved to be a powerful off-label vascular imaging agent where other agents may be contraindicated or ineffective [13–15].

In our practice at UCLA, ferumoxytol enhanced MRA (FEMRA) has been requested in growing numbers over the past eight years for patients with renal failure and in other patient groups where its advantages have become evident. In this paper, we address several clinical applications where we have found the off-label use of FEMRA effective and reliable.

Ferumoxytol compared to the extracellular GBCAs

Without doing an exhaustive dive into the physicochemical properties of the individual agents, below we highlight relevant characteristics that distinguish ferumoxytol from the broad class of extracellular GBCA.

Biodistribution and pharmacokinetics
Once injected, ferumoxytol remains unaltered in the blood with a nominal half-life of 15 hours. Its distribution volume is the blood volume, which is about 5 liters in a typical adult. It is not excreted by the kidneys or the liver and so does not appear in urine or bile. Rather, ferumoxytol is slowly taken up by white blood cells (macrophages) in liver, spleen and bone marrow and the iron is incorporated into the red blood cell synthesis pathway. The GBCAs on the other hand, once injected, begin to diffuse into the entire extracellular fluid space immediately. Their blood half-life (depending on renal function) is on the order of two minutes for the distribution phase and 90 minutes for the elimination phase [19]. The distribution volume for the GBCAs is the volume of the extracellular fluid space, which is about 15 liters in a typical adult. So, within two minutes of injection, the GBCAs become three times more diluted than ferumoxytol and their blood concentration drops further due to renal excretion. It should be noted that iron is an essential component of normal cellular metabolism, such that iron deficiency has far reaching consequences [20].

Relaxivity
The T1 relaxivity of ferumoxytol is about three times that of the currently available macrocyclic GBCAs [13, 21]. So, when coupled with its smaller distribution volume (less dilution) and slow clearance from the blood, ferumoxytol exhibits about a ten-fold advantage when compared to the GBCAs at comparable doses. The steady state distribution of ferumoxytol is established within two to five minutes of administration and thereafter uniformly high signal persists in all blood vessels and in all vascular territories.

Vascular specificity
Because ferumoxytol does not diffuse into the extravascular tissue spaces, it maintains a high gradient in concentration between blood vessels and their surroundings. This preserves the sharpness of vessel borders and makes the task of region-growing easier for post processing algorithms, such as volume rendering (VR). On the other hand, with GBCAs, once the first pass is over, enhancement of soft tissues diminishes the concentration gradient between blood vessels and their surroundings also decreases.

Image contrast basis
In addition to high T1 relaxivity, ferumoxytol also has potent T2 relaxivity [21], whereas the GBCAs do not. The T2 property can be exploited to huge advantage for black blood imaging without any requirement for magnetization preparation schemes such as double inversion or diffusion sensitization [22]. So, with appropriate image weighing, ferumoxytol can produce reliable bright blood imaging and also reliable black blood imaging. The GBCAs exhibit weak

T2 relaxivity and their T1 effects undermine black blood imaging with commonly used preparation schemes. Beyond vessel imaging, strong T2 contrast can be seen with ferumoxytol at much shorter TEs than with the GBCAs. This has relevance for improved T2-weighted imaging of solid organs, such as liver, and for susceptibility-weighted imaging in all regions, including the brain [23].

Cardiovascular imaging
For ferumoxytol in the heart, there are several noteworthy observations. Because it does not diffuse into the interstitial (extravascular) fluid space, ferumoxytol does not enhance myocardial scar. However, its intravascular fidelity could be leveraged for estimation of fractional blood volume distribution [24]. Ferumoxytol should not be used for applications such as late gadolinium enhancement, where GBCAs may have greater strengths due to their extracelullar properties. Second, ferumoxytol does not play well with TrueFISP sequences (because of its T2 effects) and the preferred cardiac cine sequence with ferumoxytol is T1 FLASH. Due to its potent and persistent shortening of the blood T1, ferumoxytol offsets the saturation that can plague non-contrast FLASH cine, such that high quality images are routinely achievable even in patient with poor cardiac function. FLASH is also relatively immune to the B_0 and B_1 non-uniformity that complicates TrueFISP cine at 3T and in patients with implanted cardiac devices [25].

Field strength compatibility
Like CEMRA with the GBCAs, FEMRA can be performed at 1.5T and 3T. Also, there is evidence of its potential at 0.5T [26].

Multi-station and repeated acquisitions
As already noted, the steady state concentration of ferumoxytol in the blood is constant. For this reason, multiple overlapping stations can be acquired reliably, without having to 'keep up with' a traveling bolus of contrast. These individual stations can then be composed into a single, large field of view image using 'Image Compose'. For the same reason, if the patient moves or does not follow breath-held instructions on the first attempt, the acquisition can be repeated with no penalty in image contrast.

Safety
Ferumoxytol is approved in the U.S. for therapy in patients with renal failure and can be used (off-label) as an alternative to the iodinated X-ray agents and the GBCAs as appropriate. The U.S. Food and Drug Administration (FDA) has warned against rapid injection of ferumoxytol due to the possibility of severe hypersensitivity reactions reported during its therapeutic use [27]. Although severe reactions have not been reported during diagnostic use of ferumoxytol [28], we strongly recommend following FDA guidelines with slow infusion and physiological monitoring. In our practice, minor infusion reactions have occurred in less than 1% of patients and in multicenter experience, mild reactions occurred in < 2% of injections [28]. Sometimes called 'Fishbane' reactions, these are self-limiting symptoms thought to be mediated through release of complement and typically manifest as chest tightness, flushing of the skin, back pain, or 'trouble taking a breath'. Whereas vital signs are stable with Fishbane reactions, without bronchospasm hypotension, tachycardia or hypoxia, they may be distressing to patients (and staff) who have not been made aware that such symptoms may occur. In that case, patients and MRI staff may become anxious and distressed and confuse the episode with severe allergy. Management is supportive and generally requires only pausing the infusion, checking vital signs and reassuring the patient. Symptoms usually resolve within five minutes, without drug intervention. Once symptoms resolve, the infusion can be restarted slowly and symptoms generally do not recur. Although our numbers are not sufficient to draw any firm conclusions about who is more or less likely to exhibit symptoms, anecdotally we have observed a cluster in young patients (four of six total were in the age range from teens to thirties) and rarity in elderly patients. Failure to recognize Fishbane reactions for what they are may result in inappropriate escalation of care and administration of potent drugs that have potentially serious side effects. If a true allergic anaphylactic reaction occurs, as it may with any injected agent, it should be managed in the same manner as other severe hypersensitivity reactions due to the GBCAs or iodinated contrast agents.

Availability
Currently, ferumoxytol is available only within the U.S. and is marketed as Feraheme (Covis Pharma GmbH, Zug, Switzerland). Within the past year, a generic version of ferumoxytol has become available in the U.S., marketed by Sandoz, a Division of Novartis (Sandoz Inc., Princeton, NJ, USA).

Clinical experience

In our experience of more than 1,500 studies in more than 1,300 patients at UCLA, ferumoxytol has been used successfully in the following broad areas:

(1) Venography: venous access mapping, central or peripheral venous occlusion, pre-operative planning for venous intervention, evaluation of the portal and hepatic venous system
(2) Arteriography: aortic aneurysm and dissections, renal transplant vascular imaging, peripheral
(3) Cardiovascular: congenital heart disease, implanted cardiac devices
(4) MRA in claustrophobic patients

Venography

Ferumoxytol in the steady state produces equivalent high contrast in both arteries and veins and MR venography with ferumoxytol is poised to set a new gold standard [29, 30].

Venous thrombosis and occlusion are increasingly frequent and potentially devastating complications of treatment in patients with malignancy and organ failure [31]. However, imaging of central veins may be impossible with ultrasound [31] and even modern CT may require high contrast doses and is prone to timing errors [32]. While non-contrast magnetic resonance venography (MRV) techniques have been applied to the central veins [33, 34], they are flow-dependent, relatively slow and are sensitive to motion artifact. Non-contrast MRV is nowadays used sparingly, outside of the brain.

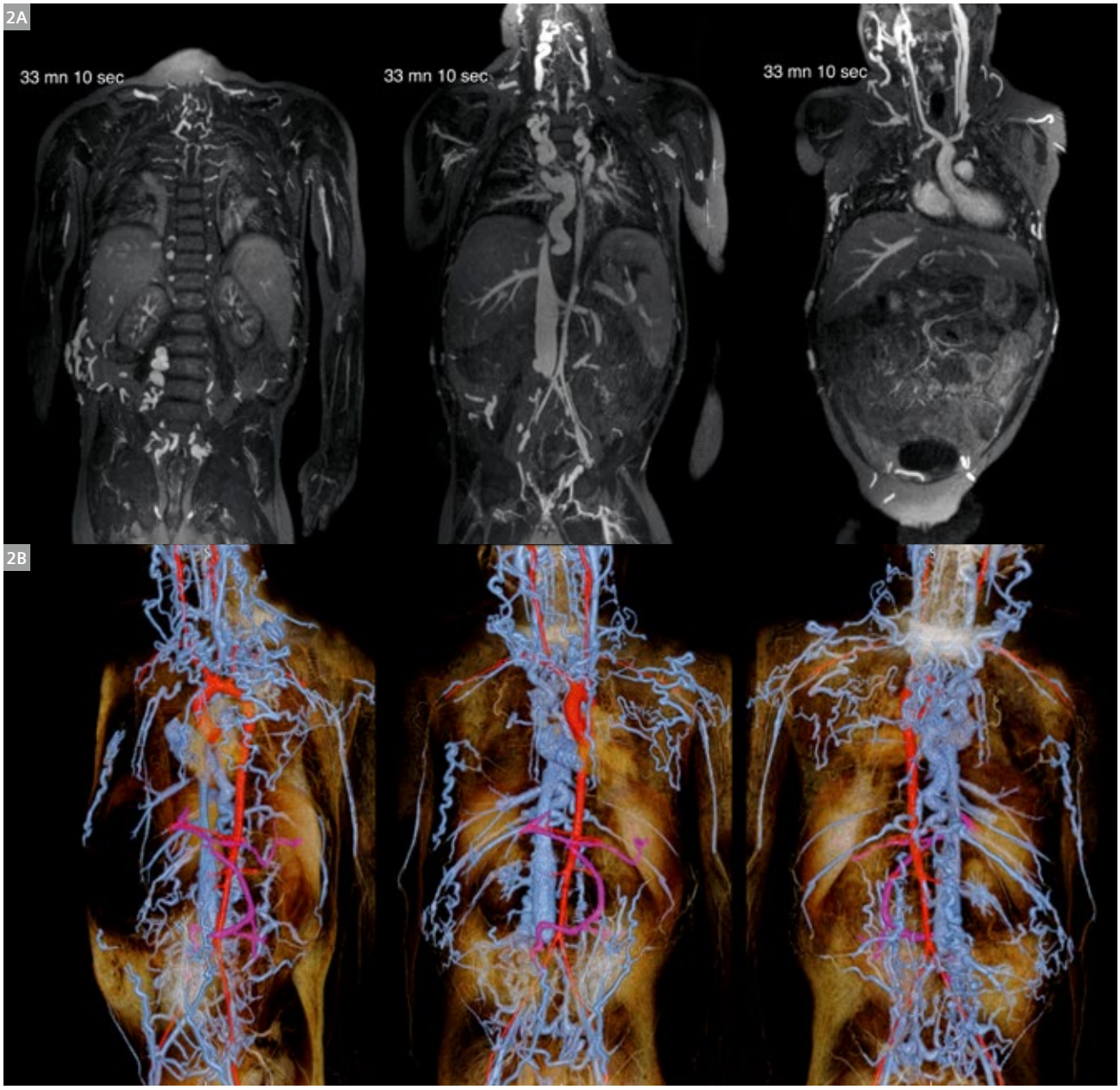

2 Ferumoxytol enhanced MRA (FEMRA) on a 3T MAGNETOM Trio a Tim system scanner in a 10-year-old boy with chronic renal failure requiring venous access. FEMRA at 30 minutes post injection show extensive venous occlusion in the chest and pelvis with extensive collateralization **(2A, B)**. Color volume rendering highlights the numerous venous collaterals (2B, blue). Systemic arteries are rendered in red and portal vein tributaries in magenta (2B). *Reproduced from [30] with permission.*

Contrast enhanced MR Venography (CEMRV) with gadolinium has been used successfully with both blood pool and extracellular agents. However, in patients with severe renal impairment, clinicians remain hesitant to request gadolinium enhanced studies, a trend exacerbated by the recent reports of gadolinium deposition in brain and bone.

Ferumoxytol is, in many ways, an ideal agent for venous imaging. Following injection, there may be great variability in the time taken for veins in different anatomic regions to enhance. Because of its long vascular half life, ferumoxytol will eventually make its way to all patent blood vessels.

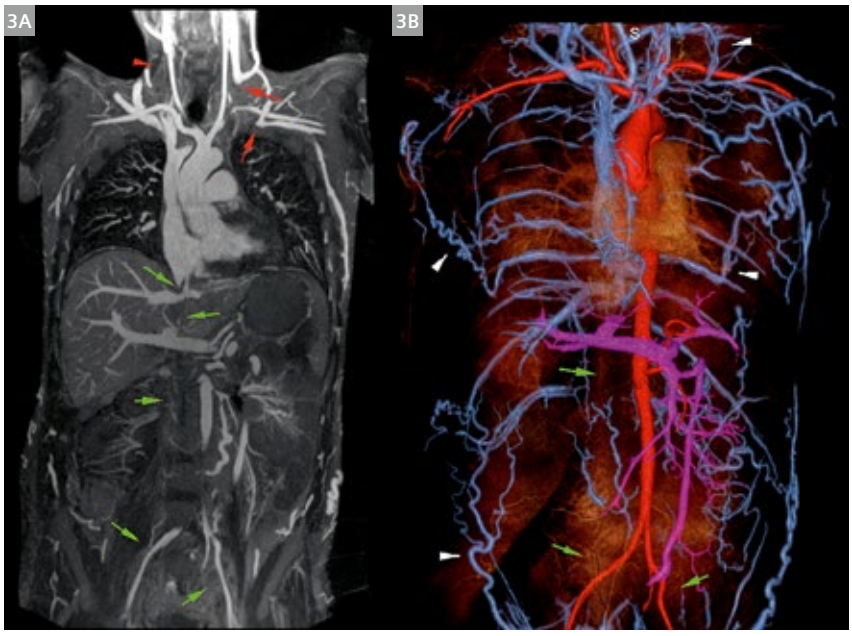

3 Ferumoxytol enhanced MRV on a 1.5T in a 33-year-old male with end-stage renal disease on hemodialysis who required venous mapping prior to central venous access. FE-MRV maximum intensity projection **(3A)** and color 3D volume rendering **(3B)** show occluded right internal jugular and subclavian veins (red arrows in 3A), non-visualized occluded right internal jugular vein (3A, red arrowhead) and complete occlusion of the entire inferior vena cava and common iliac veins (3A and B, green arrows). Collateral veins are highlighted in B (white arrowheads). The study was completed in two breath-holds, with overlapping stations in Image Compose. *Reproduced from [29] with permission.*

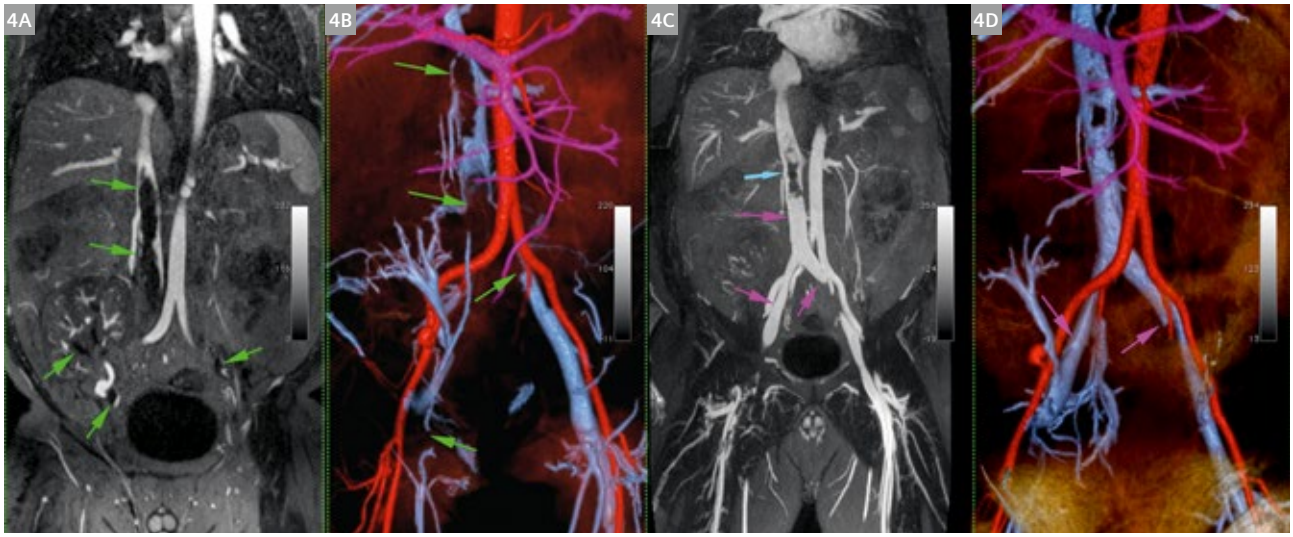

4 Ferumoxytol enhanced MRV (FEMRV) on a 1.5T in 47 year-old male with end-stage renal disease post renal transplantation presented with persistent right lower leg swelling 8 days after a filter placement in the inferior vena cava (IVC). Initial FEMRV source image **(4A)** and color 3D volume rendering **(4B)** show extensive occlusion extending from the IVC and bilateral common iliac veins to the right renal transplant vein and right common femoral vein (4A and B, green arrows). Following intervention **(4C, D)**, the IVC and common iliac veins are largely recanalized (4C and D, purple arrows) and the IVC filter (4C, blue arrow) is in good position. Single breath-hold acquisition on both occasions. *Reproduced from [29] with permission.*

No degradation in vascular contrast occurs over the entire duration of an imaging study, so venography becomes as simple as infuse, wait a few minutes and scan (Figures 1–5).

Aortic disease

For the same reasons that ferumoxytol excels at imaging the venous system, it also excels at imaging aortic aneurysms, particularly in elderly patients with tortuous vessels and slow flow. In these circumstances, bolus timing for

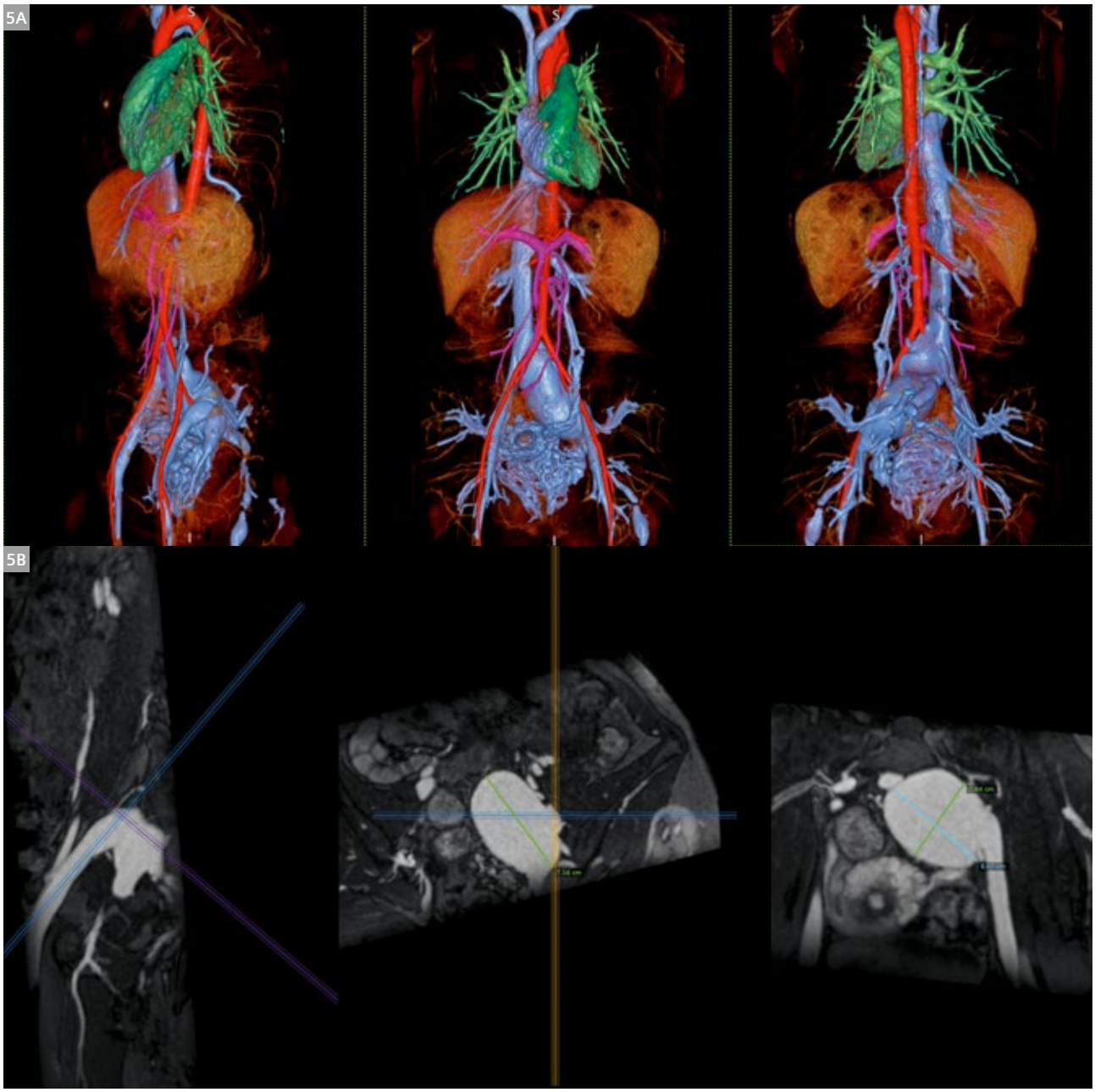

5 Ferumoxytol enhanced MRA (FEMRA) on a 3T MAGNETOM Prisma^{fit} in a 23-year-old female with giant left iliac venous aneurysm.
(5A) Color rendering from the single breath-held acquisition FEMRA shows the venous aneurysm and enlarged pelvic veins in blue.
(5B) Multiplanar reformats show dimensions of the pelvic venous aneurysm and its narrow neck.

CEMRA and for CTA can be challenging, because distal segments of the aorta may fill long after more proximal segments. With steady-state ferumoxytol, this is not an issue because contrast gains uniform access to every

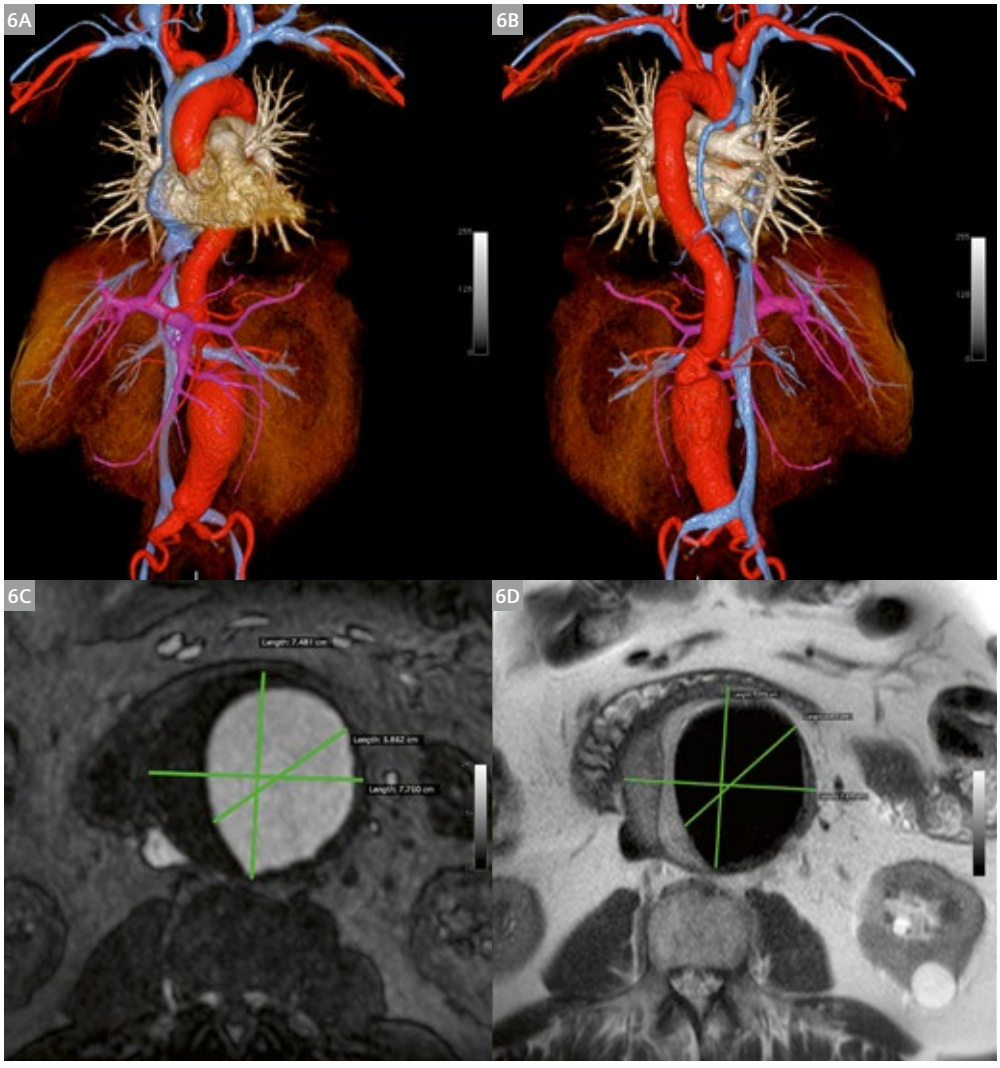

6 Ferumoxytol enhanced MRA (FEMRA) in a 65-year-old male patient with renal failure and an infra-renal abdominal aortic aneurysm being evaluated for stent graft. Color rendered, composed FEMRA **(6A, B)** show the extent of the aneurysm and include the entire aorto-iliac system. Multiplanar reformats from FEMRA **(6C)** and non-breath held HASTE **(6D)** show the dimensions of the aneurysm. The HASTE image shows differential signal from aortic plaque and mural thrombus. Note how clearly the HASTE image differentiates perfused lumen (dark) from thrombus and plaque.

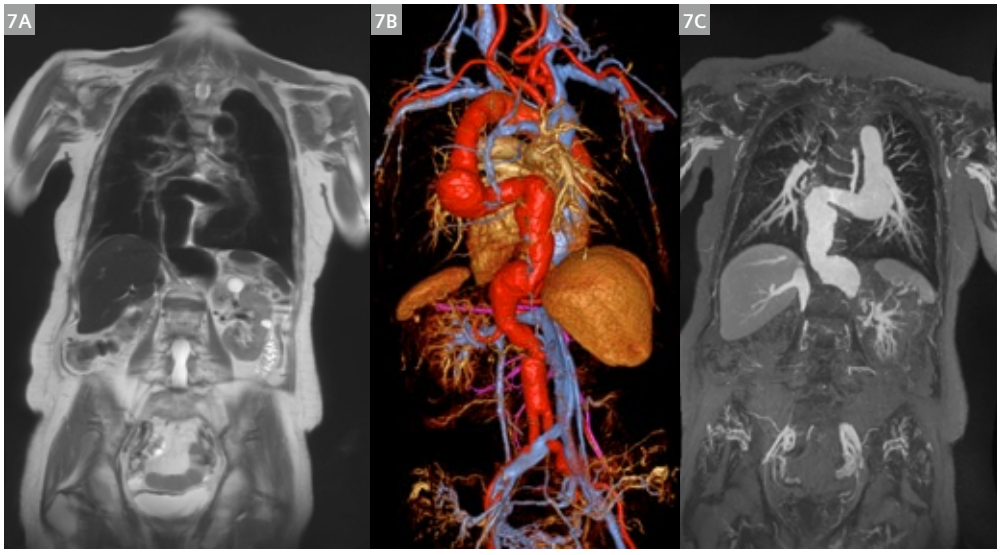

7 Ferumoxytol enhanced MRA (FEMRA) in an elderly male patient with renal failure, multi-focal, thoraco-abdominal aortic aneurysm, and prior aorto-iliac surgical graft. Color rendered, composed FEMRA **(7B)** show the extent of the aneurysm and include the entire aorto-iliac system. Multiplanar reformats from FEMRA **(7C)** and non-breath held HASTE **(7A)** show corresponding bright-blood and dark-blood images without mural thrombus.

crevice throughout the aorto-iliac system (Figures 4–8). Also, as with venous imaging, coverage can be extended with overlapping stations without loss of luminal contrast (Figures 5–8). Another advantage of ferumoxytol in aortic aneurysms is in defining mural thrombus and plaque with complementary black blood imaging (Fig. 6). This is as simple as running non-breath-held HASTE [22]. Because ferumoxytol decreases the T2 of the blood, there is no residual blood signal (or source of slow flow artifact) on HASTE, even at modest TE. Moreover, there is no requirement for black blood magnetization modules, such as double inversion or dephasing gradients. Just as the blood signal is bright on T1-weighted MRA independently of flow, the blood signal is dark on T2-weighted sequences, independently of flow.

Lower extremity MRA

Whereas steady-state imaging is fully diagnostic in the chest, abdomen and pelvis, where arteries are easily distinguished from veins, in the calves, venous enhancement can make interpretation of abnormal arterial anatomy impossible. For this reason, we have found it helpful to

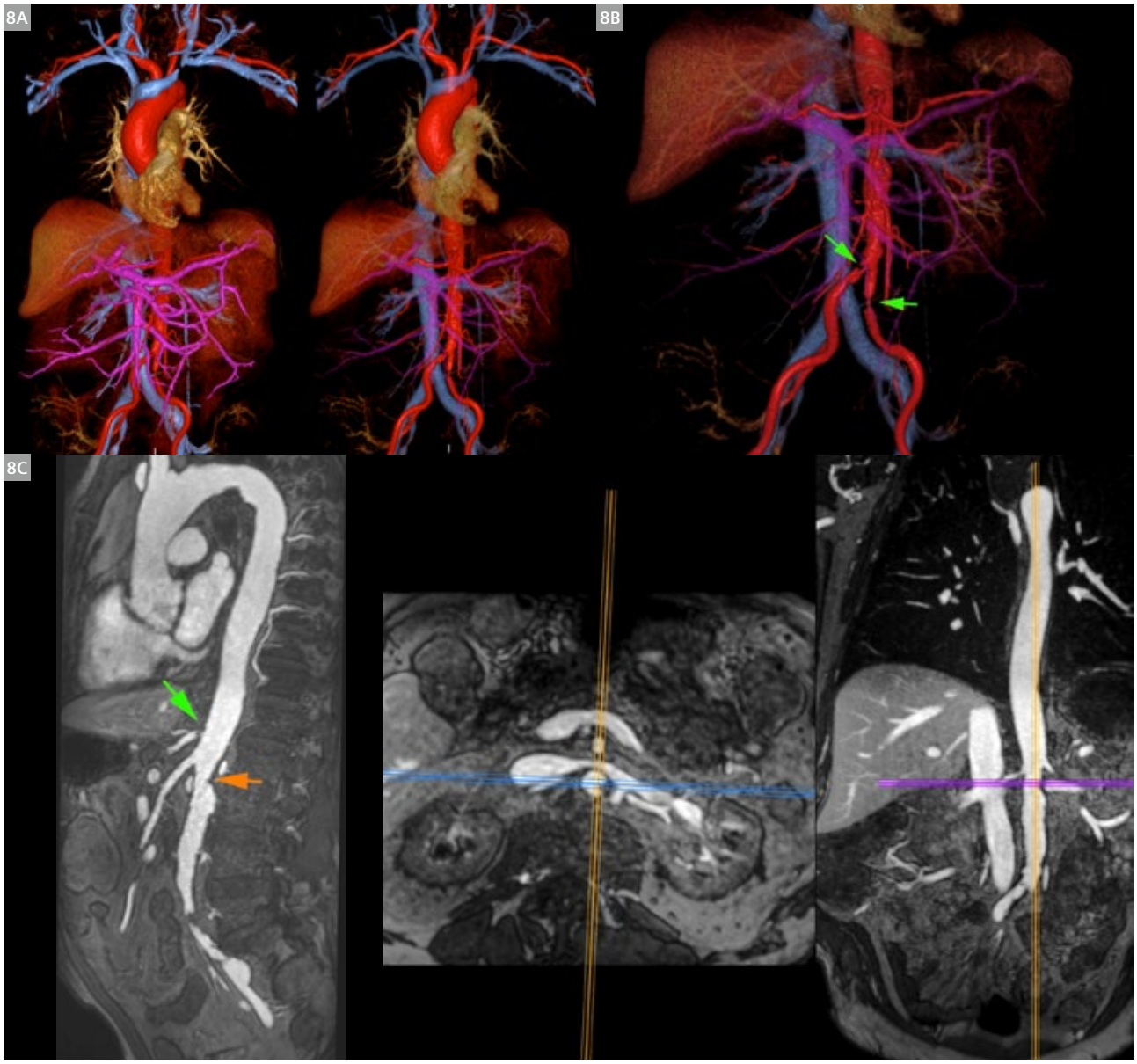

8 Ferumoxytol enhanced MRA (FEMRA) on a 3T MAGNETOM Prisma^{fit} in an 83-year-old male patient with renal failure and claudication. Panels **(8A, B)** show full field of view and focused Iliac color renderings, with severe stenoses in the common iliac arteries (green arrows). Panel **(8C)** is a multiplanar reformat through the celiac artery, showing a tight stenosis at the origin (green arrow).

inject a small dose of dilute ferumoxytol over 10 seconds and acquire TWIST images (Fig. 9) in the calves and thighs. The remaining contrast can then be infused slowly and steady state images of the chest, abdomen and pelvis acquired.

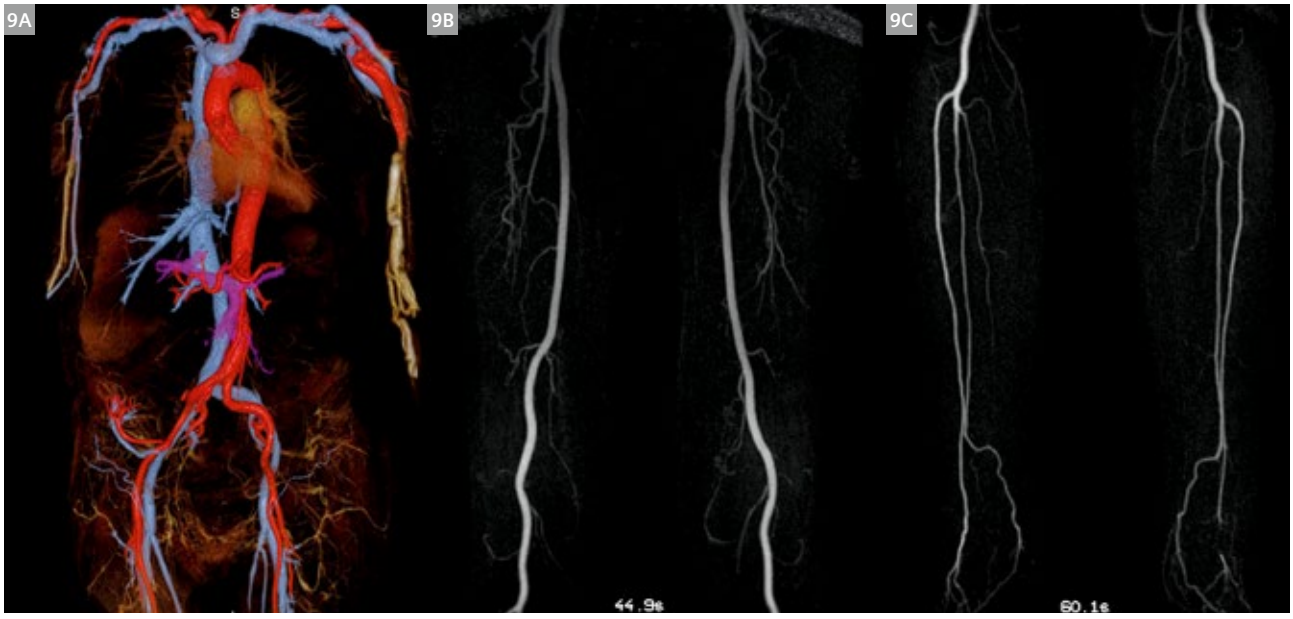

9 Ferumoxytol enhanced MRA (FEMRA) in a 75-year-old male patient with leg pain and chronic kidney disease. Low dose ferumoxytol was used for multi station dynamic TWIST imaging of the calf **(9C)** and thigh **(9B)**. Subsequently, the remaining ferumoxytol dose was infused slowly and steady state imaging of the chest, abdomen and pelvis performed (**9A**, volume rendered image shows a transplant kidney in the right pelvis).

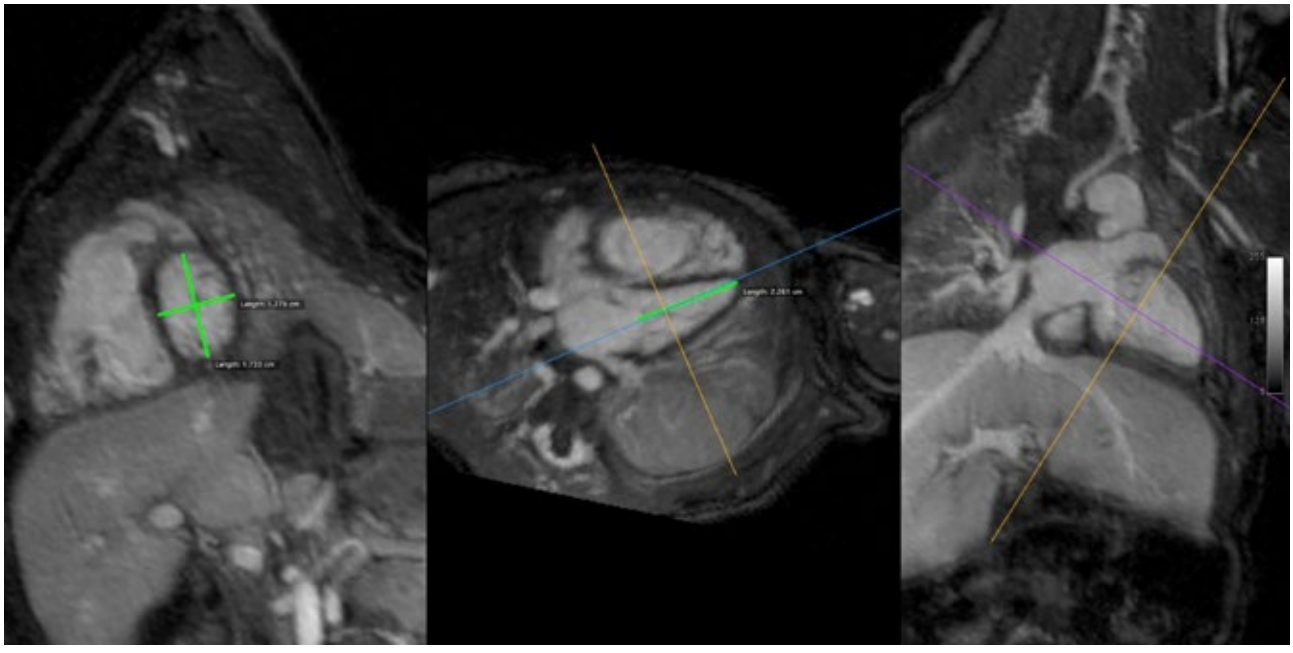

10 Ferumoxytol enhanced MRA (FEMRA) in a 2-day-old[1] neonate with suspected hypoplastic left heart syndrome. Single frame reformats from 4D MUSIC acquisition are shown. Uninterpolated voxel dimensions were 0.9 × 0.9 × 0.9 mm^3. Because of the volumetric, multi-phase acquisition, precise dimensional and volumetric measurements can be made for chamber and vessel sizes.

[1] *Siemens Healthineers Disclaimer: MR scanning has not been established as safe for imaging fetuses and infants less than two years of age. The responsible physician must evaluate the benefits of the MR examination compared to those of other imaging procedures. Note: This disclaimer does not represent the opinion of the authors.*

Pediatric congenital heart disease

In children with congenital heart disease (CHD), ferumoxytol has ushered in a paradigm shift for MRI. Because of its long half-life in the blood, ferumoxytol supports high-resolution 4D (or 5D) imaging. When implemented with both cardiac and respiratory gating, high-dimensional techniques such as MUSIC (Multiphase, Steady-state Imaging with Contrast)[2] [35–39] and free-running 3D radial imaging[3] [40] can produce images with uniformly high contrast throughout the cardiac chambers and blood vessels (Figures 10, 11). Data acquisition runs for several minutes (usually with continuous positive pressure ventilation) and images are immediately available for cine reconstruction in any plane and for comprehensive evaluation of vascular anatomy. MUSIC has proved reliable at multiple institutions and at both 1.5T and 3T [39]. The acquisition protocol is simple and reliable and is independent of the complexity of the underlying disease and anatomy.

Adult congenital heart disease (ACHD)

In adult patients with CHD, timing of a contrast bolus for evaluation of shunts such as the Fontan and Glenn can be problematic and prone to misinterpretation. Again, because of its independence from bolus timing, MRA with ferumoxytol offers huge advantages over both CTA and CEMRA in the Fontan patient. Performing MRA with cardiac gating is desirable in patients with ACHD and abnormalities involving the great vessels (Fig. 12). First pass imaging of a GBCA bolus requires that the acquisition is timed accurately both with respect to the contrast bolus arrival and the phase of the cardiac cycle. This can be a complex procedure and if either gating or bolus timing fails, the first pass opportunity is lost. With ferumoxytol in steady state, there is no bolus timing and if gating or breath-holding is suboptimal the first time, the acquisition can be repeated at leisure.

[2]MUSIC is a prototype sequence developed at UCLA.
[3]Work in progress. The application is currently under development and is not for sale in the U.S. and in other countries. Its future availability cannot be ensured.

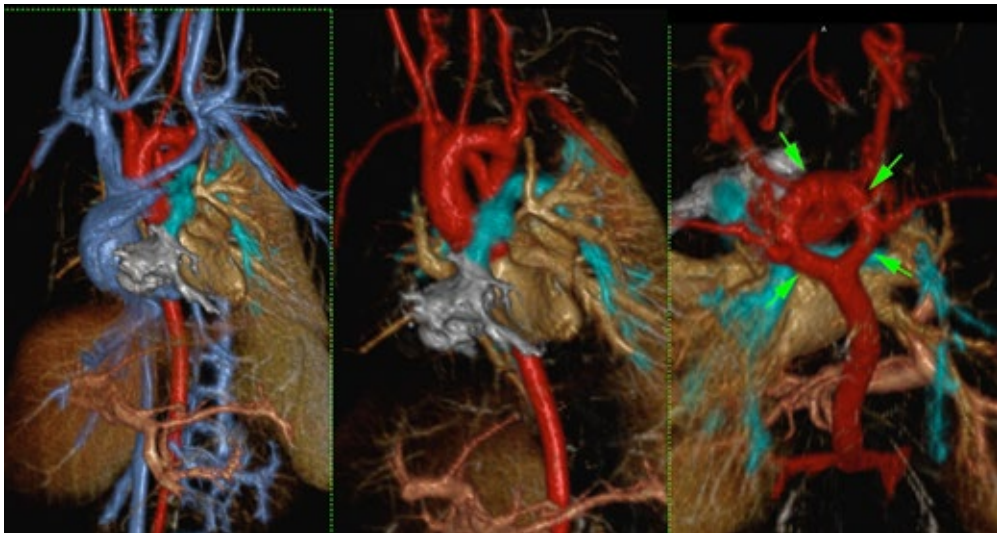

11 Ferumoxytol enhanced MRA (FEMRA) in a 6-month-old[1] male with suspected vascular ring. Single frame volume-rendered images from 4D MUSIC acquisition are shown. Uninterpolated voxel dimensions were 1.0 x 1.0 x 1.0 mm³. Color volume rendered reconstructions comprehensively show all cardiac chambers and great vessel anatomy. The double aortic arch with complete vascular ring is well shown in the right panel (arrows).

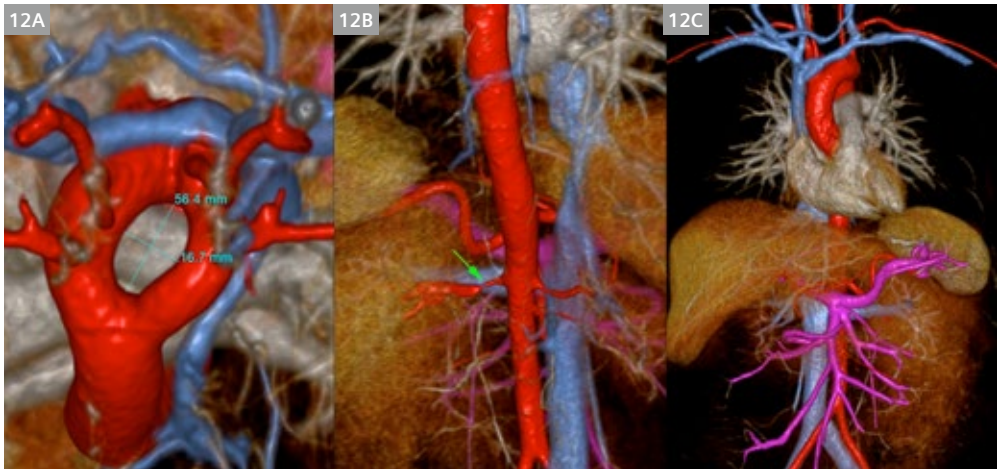

12 Ferumoxytol enhanced MRA (FEMRA) in a 48-year-old patient with double aortic arch and complete vascular ring. Color volume rendered images clearly depict a complete vascular ring and its relationship to other vessels (**12A**, viewed from above). Incidentally noted left renal artery stenosis (**12B**, arrow).

Claustrophobia

Claustrophobia of some degree is found in many patients who are otherwise suitable candidates for contrast enhanced MR angiography (CEMRA). Conventional CEMRA examinations may exceed 30 minutes within the scanner bore and patients with claustrophobia may be unwilling or unable to tolerate that. We have implemented a focused ferumoxytol-enhanced MRA (*f*-FEMRA) protocol in claustrophobic patients [41], whereby comprehensive vascular imaging can be completed in only a few minutes within the magnet bore (Fig. 13). For the *f*-FEMRA studies, where clinically appropriate, no pre-contrast imaging is performed

13 Ferumoxytol enhanced MRA (FEMRA) in a 79-year-old claustrophobic male patient with renal impairment and abdominal bruit. MIP of non-contrast CT **(13A)** and *f*-FEMRA **(13B)** show severe aortic calcification (green arrows). Note clear visualization of the perfused aortic lumen in panel 13B. *f*-FEMRA with color 3D volume rendering and an extended field of view **(13C, D)** confirm extensive distal aortic disease (13D, green arrow), stenosis of the right subclavian artery (13D, yellow arrow) and an enlarged inferior mesenteric artery forming an Arc of Riolan (13D, white arrow). Occlusion of the proximal superior mesenteric artery is highlighted in (**13E, F**, arrows). Examination time for two-station *f*-FEMRA was 6 minutes and 46 seconds. *Reproduced from [41] with permission.*

and ferumoxytol is infused outside the scanner bore (or outside the MRI suite). Automated scanner tuning and coil adjustment, without patient-specific shimming, minimizes adjustment time. Following localizers, breath-held, high resolution 3D FEMRA is performed in one or more overlapping stations. Total time within the magnet bore for *f*-FEMRA may be as little as 3 minutes.

Conclusion

The use of ferumoxytol offers many distinct advantages over conventional approaches to vascular imaging with MRI. It can simplify procedures and protocols, shorten exam durations (sometimes profoundly), improve image quality, and open up clinical applications not otherwise possible. In the examples illustrated above, we only begin to explore the potential of this versatile agent. At the time of writing, the major barriers to the more widespread use of ferumoxytol are availability, cost and the lack of an approved diagnostic label. However, none of these obstacles is insurmountable and there is growing interest in removing all of them, much to the benefit of patient care.

References

1 Napoli A, Anzidei M, Marincola BC, Zaccagna F, Geiger D, Di Paolo PL, et al. Optimisation of a high-resolution whole-body MR angiography protocol with parallel imaging and biphasic administration of a single bolus of Gd-BOPTA: preliminary experience in the systemic evaluation of atherosclerotic burden in patients referred for endovascular procedures. Radiol Med. 2009;114(4):538-52.

2 Villablanca JP, Nael K, Habibi R, Nael A, Laub G, Finn JP. 3 T contrast-enhanced magnetic resonance angiography for evaluation of the intracranial arteries: comparison with time-of-flight magnetic resonance angiography and multislice computed tomography angiography. Invest Radiol. 2006;41(11):799-805.

3 Guichet PL, Duszak R, Jr., Chaves Cerdas L, Hughes DR, Hindman N, Rosenkrantz AB. Changing National Medicare Utilization of Catheter, Computed Tomography, and Magnetic Resonance Extremity Angiography: A Specialty-focused 16-Year Analysis. Curr Probl Diagn Radiol. 2021;50(3):308-314.

4 Dodd JD, Leipsic J. Cardiovascular CT and MRI in 2019: Review of Key Articles. Radiology. 2020;297(1):17-30.

5 Mandell DM, Mossa-Basha M, Qiao Y, Hess CP, Hui F, Matouk C, et al. Intracranial Vessel Wall MRI: Principles and Expert Consensus Recommendations of the American Society of Neuroradiology. AJNR. 2017;38(2):218-229.

6 Thomsen HS. Nephrogenic systemic fibrosis: a serious adverse reaction to gadolinium - 1997-2006-2016. Part 1. Acta radiologica (Stockholm, Sweden : 1987). 2016;57(5):515-20.

7 Haneder S, Kucharczyk W, Schoenberg SO, Michaely HJ. Safety of magnetic resonance contrast media: a review with special focus on nephrogenic systemic fibrosis. Topics in magnetic resonance imaging: TMRI. 2015;24(1):57-65.

8 Malayeri AA, Brooks KM, Bryant LH, Evers R, Kumar P, Reich DS, Bluemke DA. National Institutes of Health Perspective on Reports of Gadolinium Deposition in the Brain. J Am Coll Radiol. 2016;13(3):237-41.

9 Radbruch A, Weberling LD, Kieslich PJ, Eidel O, Burth S, Kickingereder P, et al. Gadolinium retention in the dentate nucleus and globus pallidus is dependent on the class of contrast agent. Radiology. 2015;275(3):783-91.

10 Woolen SA, Shankar PR, Gagnier JJ, MacEachern MP, Singer L, Davenport MS. Risk of Nephrogenic Systemic Fibrosis in Patients With Stage 4 or 5 Chronic Kidney Disease Receiving a Group II Gadolinium-Based Contrast Agent: A Systematic Review and Meta-analysis. JAMA internal medicine. 2020;180(2):223-230.

11 Le Fur M, Caravan P. The biological fate of gadolinium-based MRI contrast agents: a call to action for bioinorganic chemists. Metallomics: integrated biometal science. 2019;20;11(2):240-254.

12 Neuwelt EA, Hamilton BE, Varallyay CG, Rooney WR, Edelman RD, Jacobs PM, Watnick SG. Ultrasmall superparamagnetic iron oxides (USPIOs): a future alternative magnetic resonance (MR) contrast agent for patients at risk for nephrogenic systemic fibrosis (NSF)? Kidney international. 2009;75(5):465-74.

13 Bashir MR, Bhatti L, Marin D, Nelson RC. Emerging applications for ferumoxytol as a contrast agent in MRI. J Magn Reson Imaging. 2015;41(4):884-98.

14 Finn JP, Nguyen KL, Han F, Zhou Z, Salusky I, Ayad I, Hu P. Cardiovascular MRI with ferumoxytol. Clin Radiol. 2016;71(8):796-806.

15 Toth GB, Varallyay CG, Horvath A, Bashir MR, Choyke PL, Daldrup-Link HE, et al. Current and potential imaging applications of ferumoxytol for magnetic resonance imaging. Kidney International. 2017;92(1):47-66.

16 Daldrup-Link HE. Ten Things You Might Not Know about Iron Oxide Nanoparticles. Radiology. 2017;284(3):616-629.

17 Prince MR, Zhang HL, Chabra SG, Jacobs P, Wang Y. A pilot investigation of new superparamagnetic iron oxide (ferumoxytol) as a contrast agent for cardiovascular MRI. Journal of X-ray science and technology. 2003;11(4):231-40.

18 Food and Drug Administration. Feraheme Label. [cited 2018 February 5]; Available from: https://www.accessdata.fda.gov/drugsatfda_docs/label/2018/022180s009lbl.pdf

19 Aime S, Caravan P. Biodistribution of gadolinium-based contrast agents, including gadolinium deposition. J Magn Reson Imaging. 2009;30(6):1259-67.

20 Lopez A, Cacoub P, Macdougall IC, Peyrin-Biroulet L. Iron deficiency anaemia. Lancet. 2016;387(10021):907-16.

21 Knobloch G, Colgan T, Wiens CN, Wang X, Schubert T, Hernando D, et al. Relaxivity of Ferumoxytol at 1.5 T and 3.0 T. Invest Radiol. 2018;53(5):257-263.

22 Nguyen KL, Park EA, Yoshida T, Hu P, Finn JP. Ferumoxytol enhanced black-blood cardiovascular magnetic resonance imaging. J Cardiovasc Magn Reson. 2017;19(1):106.

23 Buch S, Wang Y, Park MG, Jella PK, Hu J, Chen Y, et al. Subvoxel vascular imaging of the midbrain using USPIO-Enhanced MRI. Neuroimage. 2020;220:117106.

24 Colbert CM, Thomas MA, Yan R, Radjenovic A, Finn JP, Hu P, Nguyen KL. Estimation of fractional myocardial blood volume and water exchange using ferumoxytol-enhanced magnetic resonance imaging. Journal of Magnetic Resonance Imaging. 2021;53(6):1699-1709.

25 Nguyen KL YT, Hu P, Finn JP. Ferumoxytol-enhanced cardiac cine MRI in patients with implanted cardiac devices. 25th Annual ISMRM Scientific Sessions; 2017 April 22-27, 2017; Honolulu, HI, USA.

26 van Zandwijk JK, Simonis FFJ, Heslinga FG, Hofmeijer EIS, Geelkerken RH, Ten Haken B. Comparing the signal enhancement of a gadolinium based and an iron-oxide based contrast agent in low-field MRI. PloS one. 2021;16(8):e0256252.

27 Food and Drug Administration. FDA Drug Safety Communication: FDA strengthens warnings and changes prescribing instructions to decrease the risk of serious allergic reactions with anemia drug Feraheme (ferumoxytol). 2015. Available from: http://www.fda.gov/Drugs/DrugSafety/ucm440138.htm.
28 Nguyen KL, Yoshida T, Kathuria-Prakash N, Zaki IH, Varallyay CG, Finn JP, et al. Multicenter Safety and Practice for Off-Label Diagnostic Use of Ferumoxytol in MRI. Radiology. 2019;293(3):554-564.
29 Shahrouki P, Moriarty JM, Khan SN, Bista B, Kee ST, DeRubertis BG, Yoshida T, Nguyen KL, Finn JP. High resolution, 3-dimensional Ferumoxytol-enhanced cardiovascular magnetic resonance venography in central venous occlusion. J Cardiovasc Magn Reson. 2019;21(1):17.
30 Shahrouki P, Khan SN, Yoshida T, Iskander PJ, Ghahremani S, Finn JP. High-resolution three-dimensional contrast-enhanced magnetic resonance venography in children: comparison of gadofosveset trisodium with ferumoxytol. Pediatr Radiol. 2022;52(3):501-512.
31 Cushman M. Epidemiology and risk factors for venous thrombosis. Semin Hematol. 2007;44(2):62-9.
32 Ghaye B, Szapiro D, Willems V, Dondelinger RF. Pitfalls in CT venography of lower limbs and abdominal veins. AJR American journal of roentgenology. 2002;178(6):1465-71.
33 Finn JP, Zisk JH, Edelman RR, Wallner BK, Hartnell GG, Stokes KR, Longmaid HE. Central venous occlusion: MR angiography. Radiology. 1993;187(1):245-51.
34 Miyazaki M, Akahane M. Non-contrast enhanced MR angiography: established techniques. J Magn Reson Imaging. 2012;35(1):1-19.
35 Han F, Rapacchi S, Khan S, Ayad I, Salusky I, Gabriel S, Plotnik A, Finn JP, Hu P. Four-dimensional, multiphase, steady-state imaging with contrast enhancement (MUSIC) in the heart: a feasibility study in children. Magn Reson Med. 2015;74(4):1042-9.
36 Nguyen KL, Han F, Zhou Z, Brunengraber DZ, Ayad I, Levi DS, Satou GM, Reemtsen BL, Hu P, Finn JP. 4D MUSIC CMR: value-based imaging of neonates and infants with congenital heart disease. J Cardiovasc Magn Reson. 2017;19(1):40.
37 Zhou Z, Han F, Rapacchi S, Nguyen KL, Brunengraber DZ, Kim GJ, Finn JP, Hu P. Accelerated ferumoxytol-enhanced 4D multiphase, steady-state imaging with contrast enhancement (MUSIC) cardiovascular MRI: validation in pediatric congenital heart disease. NMR Biomed. 2017;30(1).
38 Han F, Zhou Z, Han E, Gao Y, Nguyen KL, Finn JP, Hu P. Self-gated 4D multiphase, steady-state imaging with contrast enhancement (MUSIC) using rotating cartesian K-space (ROCK): Validation in children with congenital heart disease. Magn Reson Med. 2017;78(2):472-483.
39 Nguyen KL, Ghosh RM, Griffin LM, Yoshida T, Bedayat A, Rigsby CK, Fogel MA, Whitehead KK, Hu P, Finn JP. Four-dimensional Multiphase Steady-State MRI with Ferumoxytol Enhancement: Early Multicenter Feasibility in Pediatric Congenital Heart Disease. Radiology. 2021;300(1):162-173.
40 Di Sopra L, Piccini D, Coppo S, Stuber M, Yerly J. An automated approach to fully self-gated free-running cardiac and respiratory motion-resolved 5D whole-heart MRI. Magn Reson Med. 2019;82(6):2118-2132.
41 Shahrouki P, Nguyen KL, Moriarty JM, Plotnik AN, Yoshida T, Finn JP. Minimizing table time in patients with claustrophobia using focused ferumoxytol-enhanced MR angiography (*f*-FEMRA): a feasibility study. Br J Radiology. 2021;94(1125):20210430.

Contact

J. Paul Finn, M.D.
Department of Radiological Sciences
University of California Los Angeles
Peter V. Ueberroth Building, Suite 3371
10945 Le Conte Ave
Los Angeles, CA 90095-7206
USA
pfinn@mednet.ucla.edu

3D Whole Heart Applications: Angiography and Delayed Enhancement

Jason Craft[1], Joshua Y. Cheng[1], Nancy Diaz[1], Karl P. Kunze[2], Michaela Schmidt[3]

[1]St. Francis Heart Hospital, DeMatteis Research Center, Greenvale, NY, USA
[2]Siemens Healthcare Limited, Frimley, UK
[3]Siemens Healthineers, Erlangen, Germany

Introduction

It has become more important than ever before to diversify non-invasive imaging methods that involve contrast media administration. Compared to CT imaging, MRI does not involve nephrotoxic iodinated contrast or ionizing radiation. However, ungated first pass magnetic resonance angiography (MRA) cannot effectively freeze cardiac motion; and provides reduced quality of segmentation compared to CT pulmonary vein angiography [1]. Diaphragmatic navigator (dNAV) used for motion correction is associated with unpredictable scan times when respiration is irregular, and imperfect slab tracking ratio [2]. Furthermore, approximately 50–100 Hz off-resonance is frequently observed at the interface of the pulmonary veins and left atrium due to susceptibility effects and inflow from the lungs [3]. Therefore, the use of balanced steady-state free precession (bSSFP) and fat saturation pulses, particularly at higher field strengths, can be technically unsatisfactory for this application. Thus, the unmet clinical need is to provide robust clinical angiographic methods that can effectively image complex patients with arrhythmias, while minimizing image artifacts.

Instead of tracking the diaphragmatic interface, image navigators (iNAV) track the blood pool contrast of the left ventricle [4]. 2D translational motion in the head-to-foot direction can be extracted and estimated on a per cardiac cycle basis and is used to bin data with

Imaging parameters for whole heart MRA and LGE			
Sequence	Inversion recovery GRE	Saturation recovery GRE	Inversion recovery Dixon GRE
FOV	320 mm (axial)	320 mm (axial)	320 mm (axial)
Spatial resolution	1.3 × 1.3 mm	1.3 × 1.3 mm	1.3 × 1.3 mm
Slice thickness	1.4 mm	1.4 mm	1.4 mm
Slice resolution	90%	90%	90%
Fat Sat	No	Yes	No
Acceleration Factor	2.9	2.9	2.8
Bandwidth	579 Hz/px	579 Hz/px	453 Hz/px
Flip angle	18°	18°	15°
TI/Saturation time	220–260 ms (systolic) 290 ms (diastolic)	150 ms	According to scout
TE/TR	1.42 ms/3.89 ms	1.42 ms/3.89 ms	2.38, 4.76 ms/6.97 ms
Data window duration	62–130 ms	62–130 ms	62–130 ms

Table 1: 3D whole heart sequence parameters.

respect to respiration. 3D image volumes are obtained using a non-rigid motion-compensated reconstruction of all binned data [5, 6], leading to 100% scan efficiency and predictable scan time. The sampling pattern consists of spiral-like interleaves acquired alternately based on the golden angle of rotation (variable-density golden-step Cartesian trajectory with spiral profile order sampling, or VD-CASPR)[1] [7].

As a result of scanning more efficiently, the predictable scan time translates into less gadolinium-based contrast agent (GBCA) use. Specifically, compared to dNAV based applications, we can use 33% less contrast [8, 9], and we can do it without the need for higher field strengths. Furthermore, we can acquire angiography and delayed enhancement at higher near isotropic spatial resolution. We acquire all 3D datasets at a true spatial resolution of $1.3 \times 1.3 \times 1.5$ mm^3, with a reconstructed slice thickness of 1.4 mm (Table 1).

Pulmonary vein angiography and arterial delayed enhancement using iNAV

At our institution, we are asked to provide pulmonary vein anatomical imaging for segmentation and importation into the electro-anatomical mapping system. With MRI, not only is anatomical information obtained, but functional information such as atrial and ventricular volumetrics, left atrial delayed enhancement, and quantification of valvular heart disease. Obtaining one MRI examination is simply more logistically efficient than obtaining CT angiography plus echocardiography imaging. Our 3D MRA and late gadolinium enhancement (LGE) imaging is performed on a 1.5T MAGNETOM Sola, but our institution also has experience with the 3D inversion recovery Dixon multi-echo gradient recalled echo (GRE)[1] performed on the 3T MAGNETOM Skyra platform.

Concerning the MRA and LGE exam workflow, the image navigator and saturation band position can be automatically determined using free-breathing 3 plane localizers and the AI cardiac scan companion (AICSC)[1] prototype. The diastolic or systolic rest period of the left atrium can be determined using the included high temporal resolution free breathing 4-chamber (or HLA) cine [10]. The user can manually determine the data window duration, or this can be automatically determined based on the rest period of the right coronary artery by the AICSC. Given the diastolic rest period is longer at slower ventricular rates, we prefer diastolic imaging at regular heart rhythms < 80 BPM. When the ventricular rate is > 80 BPM or significant arrhythmia such as atrial fibrillation is present, systolic imaging is preferential.

In addition to the prototype sequence[1] for *syngo* XA20 featuring 3D inversion recovery Dixon multi-echo GRE, 3D T2 prep bSSFP, and 3D T2 Prep Dixon multi-echo GRE, the user can configure different preparatory pulses to manipulate image contrast. We acquire pulmonary vein angiography using either inversion recovery GRE or saturation recovery GRE. Both methods have respective strengths and weaknesses. Inversion recovery maintains vessel sharpness and is compatible with the 1500 Hz wideband pulse which mitigates device artifacts. Furthermore, inversion recovery can be used without fat saturation, which makes this option especially attractive at higher field strengths. The inversion time parameter at 1.5T represents a balance between SNR and background suppression-values range from 220 ms to 300 ms at 1.5T [11–14]. Similar to previous literature [15], we have observed that image contrast is quite consistent even with irregular rhythms; iNAV tracking similarly remains quite robust despite the dependence of the beat-to-beat image contrast on the RR interval. Figure 1 depicts excellent image quality despite underlying atrial fibrillation, using inversion recovery GRE. Saturation recovery images have overall higher signal-to-noise, and can be used without manipulation of the inversion time parameter.

Simplifying the contrast injection scheme is important to reduce human error and to optimize workflow. Our contrast injection scheme does not involve the use of look-up tables, saline dilution, or manipulation of extra tubing and/or stop cocks. To provide adequate signal for iNAV tracking, 0.05 mmol/kg of 1 molar contrast agent is injected at 2 ml/sec, followed by 20 ml of saline at the same rate. Immediately after, the remaining 0.10 mmol/kg contrast is administered as a slow infusion, followed by saline at the same rate (0.2 ml/sec). The contrast is injected after starting the first 3D scan, and after observing satisfactory cardiac gating and appropriate iNAV placement prescription. This scan is solely run for the iNAV functionality in order to visualize contrast passage and arrival. The first, second pass, and continuous infusion dose is observed passing through the heart (Fig. 2). The first 3D scan is stopped as soon as the contrast peaks in the pulmonary artery. The exact same protocol is restarted by using STOP/CONTINUE on the inline display (which was linked by the copy reference "copy everything"). We target a maximum scan duration of 4 minutes given the length of the contrast administration and need to perform other imaging prior to delayed enhancement. 15 minutes after the initial injection of GBCA, we perform delayed enhancement of the left atrium using the inversion recovery Dixon multi-echo GRE whole heart sequence at identical spatial resolution. If desired, residual fat can be subtracted from the 3D MRA using the inversion recovery Dixon multi-echo.

[1] *Work in progress. The application is currently under development and is not for sale in the U.S. and in other countries. Its future availability cannot be ensured.*

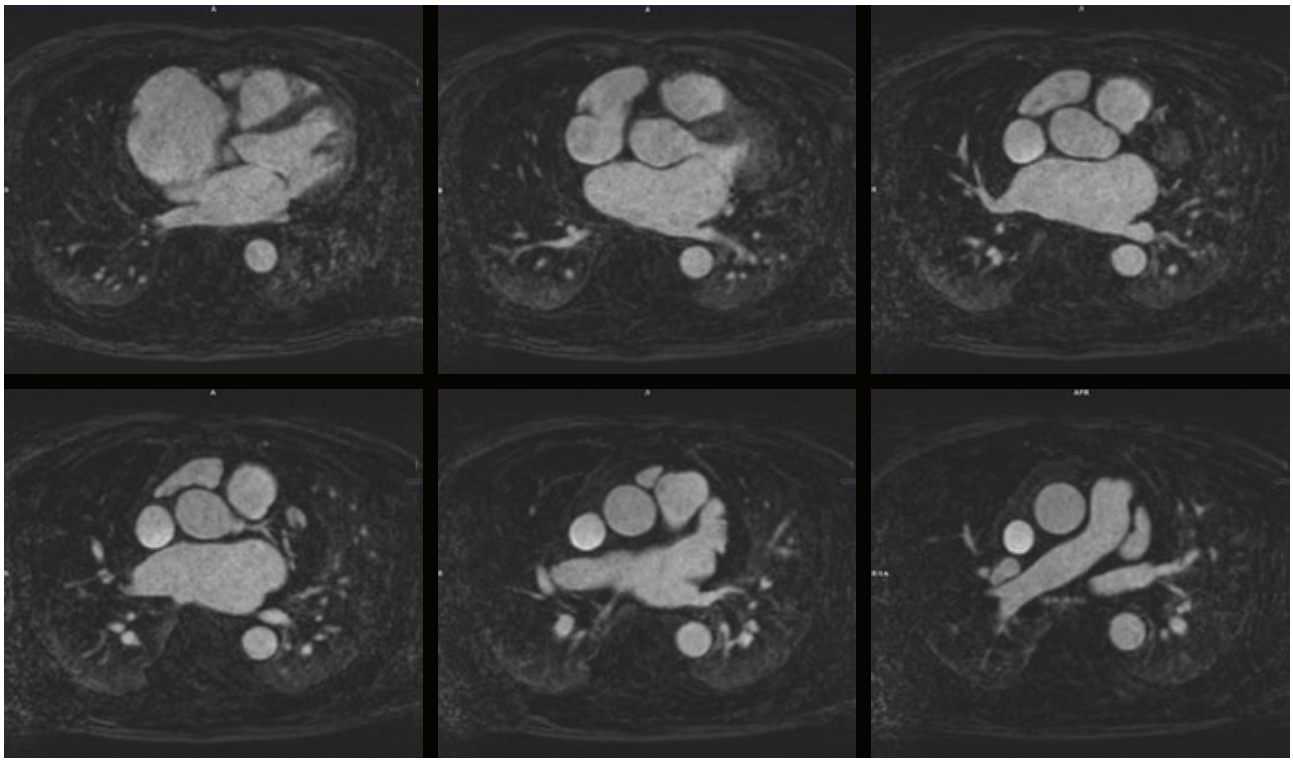

1 3D whole heart MRA inversion recovery subtracted images from a patient in atrial fibrillation.

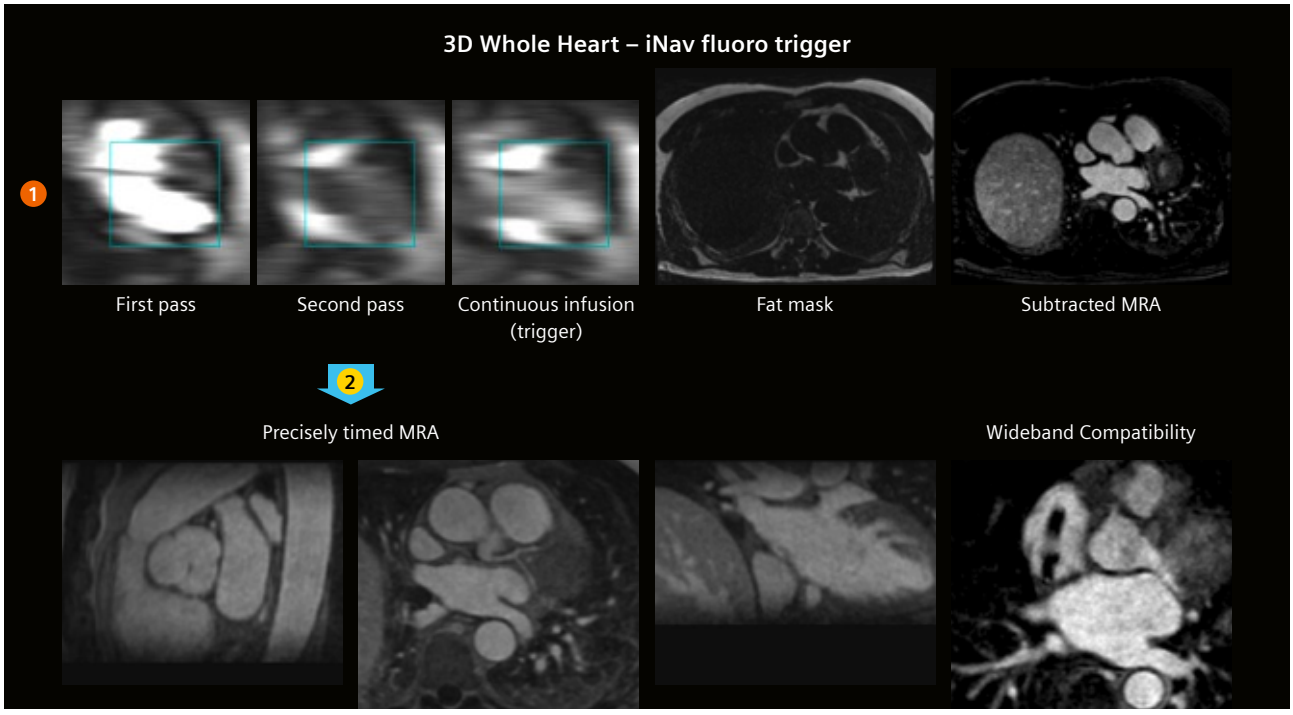

2 The iNAV fluoro trigger method for MR angiography. Two identical 3D whole heart program steps are created in the workflow. The first step (1) is used only for monitoring the passage of contrast with the iNAV. The second step (2), which will run to completion, is triggered at the peak of the continuous infusion in the pulmonary artery.

GRE fat image as a mask. As mentioned, because of the scan efficiency of the iNAV and precision timing of the contrast infusion, we are able to reduce contrast from 0.20 mmol/kg to 0.15 mmol/kg while still providing robust image quality whether patient is in sinus rhythm or has atrial fibrillation.

Case 1

A 59-year-old male was referred for evaluation of COVID-19 myocarditis and to evaluate the left atrial appendage. The patient contracted COVID-19 three weeks prior; one week prior to cardiac MRI imaging, the patient had new onset atrial fibrillation and dyspnea on exertion. Ventricular function with bSSFP cine demonstrated enlargement of the right ventricle with mildly reduced systolic function. Revised Lake Louise criteria was not met for acute myocarditis; however the patient had bilateral pulmonary emboli involving the right middle, right upper, right lower, and left lower segmental branches, with thrombus extending into the right main pulmonary artery. There was no evidence of left atrial appendage thrombus. Figure 3 illustrates the findings on 3D whole heart saturation recovery angiography and inversion recovery Dixon multi-echo GRE. Subsequent CT pulmonary angiogram agreed with MRI findings, and ultrasound Doppler was positive for

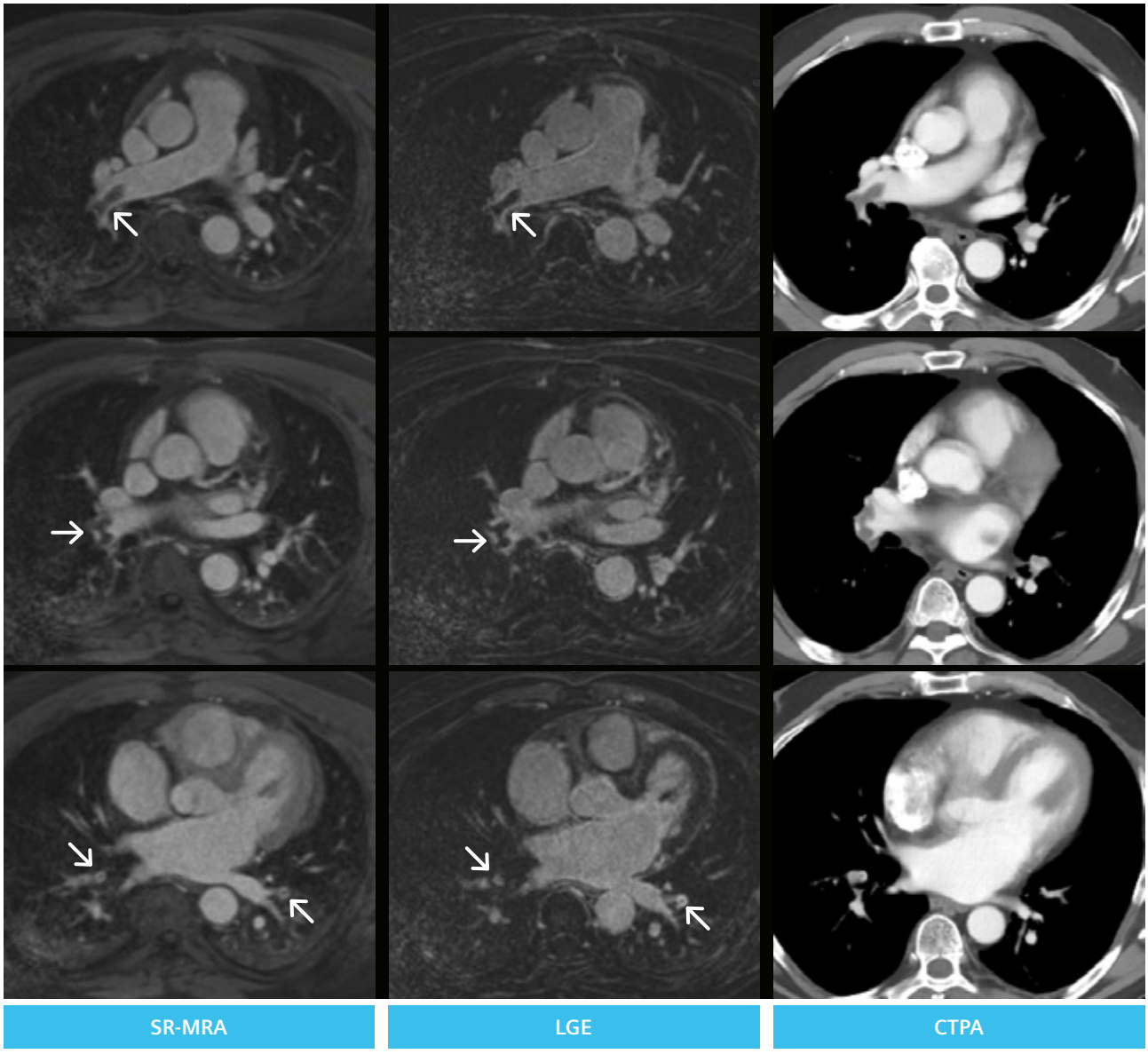

3 Incidentally discovered bilateral pulmonary emboli (arrowheads). From left to right column: saturation recovery MRA, inversion recovery Dixon multi-echo GRE, and CT pulmonary angiography.

acute right popliteal deep venous thrombosis. It is important to understand that CT pulmonary venography is timed to opacification of the left atrium; therefore abnormalities involving the pulmonary arteries may be incompletely characterized. Imaging with 3D whole heart, however, does not suffer from this limitation.

3D left ventricular delayed enhancement

In most cases, 2D PSIR LGE can provide sufficient detail and quantification of left ventricular scar burden. However there are clinical scenarios where providing a 3D dataset is beneficial, such as pre-planning for electrophysiology procedures, or for improved visualization of the right ventricle [16]. Specifically, 3D high resolution LGE can identify substrate features that may be subtle or absent on 2D imaging. By acquiring these 3D datasets in high resolution and reduced partition thickness we can minimize partial volume effects, allow for visualization of heterogeneity within regions of enhancement, scar channels, and the presence of epicardial components. Here, the user has flexible options: the 3D inversion recovery Dixon multi-echo GRE which provides more robust fat separation and is most beneficial at 3T; whereas fat saturated inversion recovery GRE can be used for scan efficiency at 1.5T. Both methods are compatible with the 1500 Hz wideband pulse which suppresses metallic artifacts caused by implanted devices such as ICDs or pacemakers.[2]

Case 2

A 67-year-old male referred for evaluation of non-sustained ventricular tachycardia (NSVT). The patient has frequent ventricular arrhythmia throughout the study, and ventricular function was only possible by using compressed sensing real time cine. Whole heart inversion recovery with fat sat LGE demonstrates heterogenous inferolateral scar with clear borders, scar channels, and epicardial component. A transmural segment of enhancement is also demonstrated in the mid anterolateral wall. 3D LGE with a restrictive temporal window is able to capture small and relevant details missing in the traditional 2D approach. This is only possible due to the 100% efficiency of the iNAV since we can trade acquisition efficiency for a smaller data acquisition window. In contrast, 2D PSIR LGE effectively freezes cardia

[2]The MRI restrictions (if any) of the metal implant must be considered prior to patient undergoing MRI exam. MR imaging of patients with metallic implants brings specific risks. However, certain implants are approved by the governing regulatory bodies to be MR conditionally safe. For such implants, the previously mentioned warning may not be applicable. Please contact the implant manufacturer for the specific conditional information. The conditions for MR safety are the responsibility of the implant manufacturer, not of Siemens Healthineers.

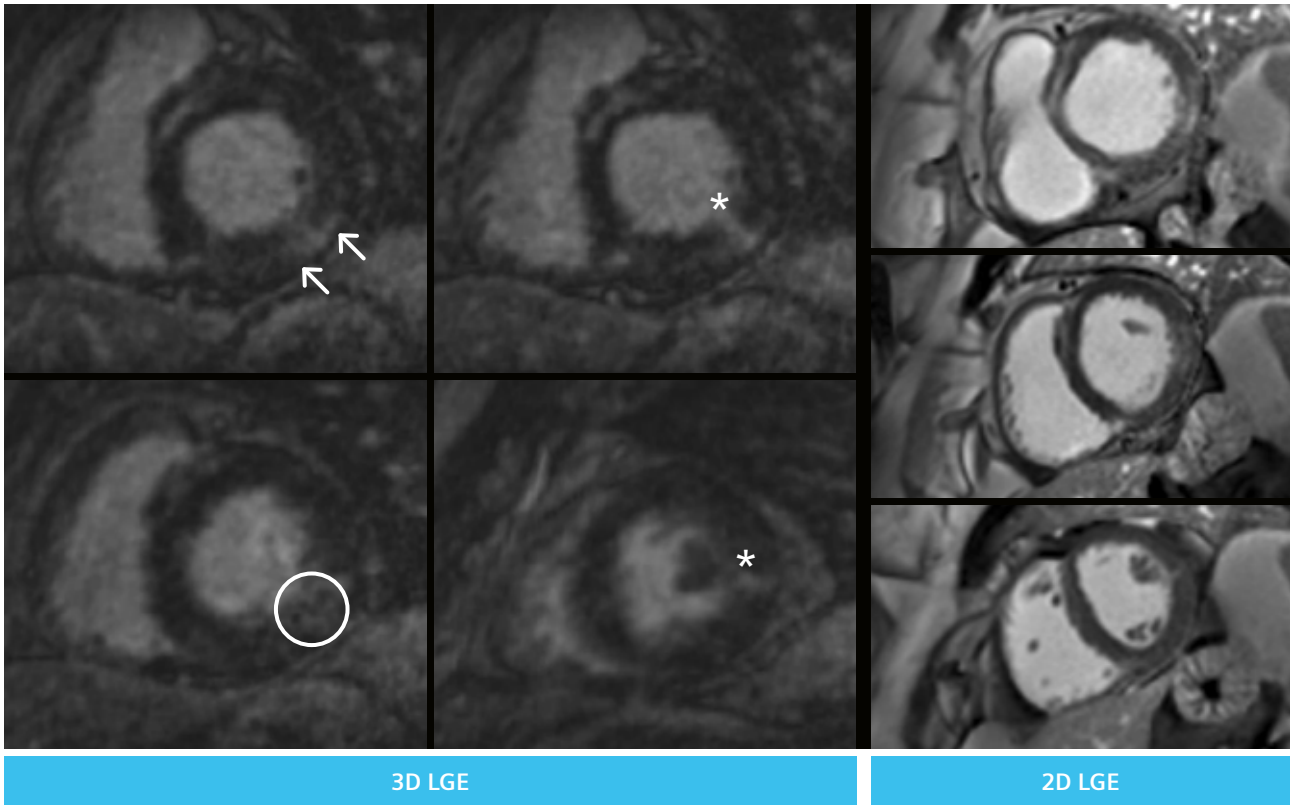

4 Comparison of 3D LGE vs 2D LGE. 3D LGE clearly demonstrates a heterogenous rim-like area of enhancement (circle), scar channels (asterisks), and epicardial component to scar (arrows). Features are ill-descript on 2D LGE.

motion, but incompletely characterizes respective areas of enhancement (Fig. 4).

Summary

In addition to what has already been described in this article, the potential for 3D whole heart to similarly accelerate coronary MRA has also been explored [17]. Submillimeter isotropic spatial resolution, with faithful representation of detail compared with the fully sampled reference can be obtained in a fraction of the time. Likewise, whole chest non-contrast MRA can be acquired more efficiently with 3D T2 prep fat saturated bSSFP at 1.5T [18] or using 3D T2 prep Dixon GRE at 3T. In conclusion, 3D whole heart is a versatile and robust package that overcomes the limitations of traditional dNAV methods for motion correction, combining VD-CASPR and iNAVs for acquisition and SNR efficiency as well as predictable scan time. Furthermore, AI based automatic positioning features and rest period scout facilitate ease of use for new and experienced users alike.

References

1 Dong J, Dickfeld T, Dalal D, Cheema A, Vasamreddy CR, Henrikson CA, Marine JE, Halperin HR, Berger RD, Lima JA, Bluemke DA, Calkins H. Initial experience in the use of integrated electroanatomic mapping with three-dimensional MR/CT images to guide catheter ablation of atrial fibrillation. J Cardiovasc Electrophysiol. 2006;17: 459-66.

2 Moghari MH, Hu P, Kissinger KV, Goddu B, Goepfert L, Ngo L, Manning WJ, Nezafat R. Subject-specific estimation of respiratory navigator tracking factor for free-breathing cardiovascular MR. Magn Reson Med. 2012;67(6):1665-72.

3 Hu P, Peters DC, Stoeck C, Kissinger KV, Goddu B, Goepfert L, Manning WJ, Nezafat R. Off-resonant pulmonary vein imaging. J Cardiovasc Magn Reson. 2009;11(Suppl 1):P185.

4 Henningsson M, Koken P, Stehning C, Razavi R, Prieto C, Botnar RM. Whole-heart coronary MR angiography with 2D self-navigated image reconstruction. Magn Reson Med. 2012;67(2):437-45.

5 Cruz G, Atkinson D, Henningsson M, Botnar RM, Prieto C. Highly efficient nonrigid motion-corrected 3D whole-heart coronary vessel wall imaging. Magn Reson Med. 2017;77(5):1894-1908.

6 Zeilinger MG, Kunze KP, Munoz C, Neji R, Schmidt M, Croisille P, Heiss R, Wuest W, Uder M, Botnar RM, Treutlein C, Prieto C. Non-rigid motion-corrected free-breathing 3D myocardial Dixon LGE imaging in a clinical setting. Eur Radiol. 2022;32(7):4340-4351.

7 Munoz C, Bustin A, Neji R, Kunze KP, Forman C, Schmidt M, Hajhosseiny R, Masci PG, Zeilinger M, Wuest W, Botnar RM, Prieto C. Motion-corrected 3D whole-heart water-fat high-resolution late gadolinium enhancement cardiovascular magnetic resonance imaging. J Cardiovasc Magn Reson. 2020;22(1):53.

8 Bustin A, Sridi S, Gravinay P, Legghe B, Gosse P, Ouattara A, Rozé H, Coste P, Gerbaud E, Desclaux A, Boyer A, Prevel R, Gruson D, Bonnet F, Issa N, Montaudon M, Laurent F, Stuber M, Camou F, Cochet H. High-resolution Free-breathing late gadolinium enhancement Cardiovascular magnetic resonance to diagnose myocardial injuries following COVID-19 infection. Eur J Radiol. 2021;144:109960.

9 Tandon A, James L, Henningsson M, Botnar RM, Potersnak A, Greil GF, Hussain T. A clinical combined gadobutrol bolus and slow infusion protocol enabling angiography, inversion recovery whole heart, and late gadolinium enhancement imaging in a single study. J Cardiovasc Magn Reson. 2016;18(1):66.

10 Yoon SS, Hoppe E, Schmidt M, Forman C, Chitiboi T, Sharma P, Tillmanns C, Maier A, Wetzl JA. Robust Deep-Learning-based Automated Cardiac Resting Phase Detection: Validation in a Prospective Study. Proc Intl Soc Mag Reson Med. 2020;28:2210.

11 Dabir D, Naehle CP, Clauberg R, Gieseke J, Schild HH, Thomas D. High-resolution motion compensated MRA in patients with congenital heart disease using extracellular contrast agent at 3 Tesla. J Cardiovasc Magn Reson. 2012;14:75.

12 Lam CZ, Pagano JJ, Gill N, Vidarsson L, de la Mora R, Seed M, Grosse-Wortmann L, Yoo SJ. Dual phase infusion with bolus tracking: technical innovation for cardiac and respiratory navigated magnetic resonance angiography using extracellular contrast. Pediatr Radiol. 2019;49(3):399-406.

13 Febbo JA, Galizia MS, Murphy IG, Popescu A, Bi X, Turin A, Collins J, Markl M, Edelman RR, Carr JC. Congenital heart disease in adults: Quantitative and qualitative evaluation of IR FLASH and IR SSFP MRA techniques using a blood pool contrast agent in the steady state and comparison to first pass MRA. Eur J Radiol. 2015;84(10):1921-1929.

14 Zheng J, Bae KT, Woodard PK, Haacke EM, Li D. Efficacy of slow infusion of gadolinium contrast agent in three-dimensional MR coronary artery imaging. J Magn Reson Imaging. 1999;10(5):800-805.

15 Groarke JD, Waller AH, Vita TS, Michaud GF, Di Carli MF, Blankstein R, Kwong RY, Steigner M. Feasibility study of electrocardiographic and respiratory gated, gadolinium enhanced magnetic resonance angiography of pulmonary veins and the impact of heart rate and rhythm on study quality. J Cardiovasc Magn Reson. 2014 ;16(1):43.

16 Ghonim S, Ernst S, Keegan J, Giannakidis A, Spadotto V, Voges I, Smith GC, Boutsikou M, Montanaro C, Wong T, Ho SY, McCarthy KP, Shore DF, Dimopoulos K, Uebing A, Swan L, Li W, Pennell DJ, Gatzoulis MA, Babu-Narayan SV. Three-Dimensional Late Gadolinium Enhancement Cardiovascular Magnetic Resonance Predicts Inducibility of Ventricular Tachycardia in Adults With Repaired Tetralogy of Fallot. Circ Arrhythm Electrophysiol. 2020;13(11):e008321.

17 Bustin A, Ginami G, Cruz G, Correia T, Ismail TF, Rashid I, Neji R, Botnar RM, Prieto C. Five-minute whole-heart coronary MRA with sub-millimeter isotropic resolution, 100% respiratory scan efficiency, and 3D-PROST reconstruction. Magn Reson Med. 2019;81(1):102-115.

18 Hajhosseiny R, Rashid I, Bustin A, Munoz C, Cruz G, Nazir MS, Grigoryan K, Ismail TF, Preston R, Neji R, Kunze K, Razavi R, Chiribiri A, Masci PG, Rajani R, Prieto C, Botnar RM. Clinical comparison of sub-mm high-resolution non-contrast coronary CMR angiography against coronary CT angiography in patients with low-intermediate risk of coronary artery disease: a single center trial. J Cardiovasc Magn Reson. 2021;23(1):57.

Contact

Jason Craft, M.D.
Department of Cardiovascular Imaging
St. Francis Heart Hospital
DeMatteis Research Center
101 Northern Blvd
Greenvale NY, 11548
USA
Jason.craft@chsli.org

High Spatial Resolution Coronary Magnetic Resonance Angiography: A Single Center Experience

Reza Hajhosseiny[1]; Aurélien Bustin[1]; Imran Rashid[1]; Gastao Cruz[1]; Karl P. Kunze[1,2]; Radhouene Neji[1,2]; Ronak Rajani[3]; Claudia Prieto[1]; René M. Botnar[1]

[1]School of Biomedical Engineering and Imaging Sciences, King's College London, London, United Kingdom
[2]MR Research Collaborations, Siemens Healthcare Limited, Frimley, United Kingdom
[3]School of Cardiovascular Medicine and Sciences, King's College London, London, United Kingdom

Abstract

Coronary magnetic resonance angiography (CMRA) could potentially offer a safe, non-invasive alternative for the anatomical assessment of coronary artery disease (CAD), which is free of ionizing radiation and iodinated contrast agents. However, image acquisition with conventional free-breathing CMRA frameworks is limited by long and unpredictable scan times, whilst image degradation due to respiratory motion remains a challenge. Here we outline a CMRA framework, that aims to overcome some of these challenges by incorporating a highly undersampled Cartesian acquisition with a two-dimensional (2D) image navigator to enable 100% respiratory scan efficiency, 2D translational motion correction, and three-dimensional (3D) non-rigid motion estimation, which is then fully reconstructed using a 3D patch-based low-rank regularization framework (PROST)[1]. We recently validated this framework against coronary computed tomography angiography (CCTA) in a single-center trial of 50 patients with suspected CAD. Diagnostic image quality was obtained in 95% of all coronary segments. The sensitivity, specificity, and negative predictive value were as follows: per-patient, 100%, 74%, and 100%; per-vessel, 81%, 88%, and 97%; and per-segment, 76%, 95%, and 99%, respectively. These findings emphasize the growing potential of this CMRA framework as a viable alternative to CCTA and invasive X-ray angiography for the anatomical assessment of CAD.

Introduction

Cardiovascular disease is the leading cause of mortality worldwide [1]. Among all causes of cardiovascular disease, atherosclerotic coronary artery disease (CAD) accounts for approximately half of all cases [1]. The early detection and long-term monitoring of CAD enable targeted risk stratification and prophylactic treatment of patients most at risk of progressing toward acute coronary syndromes. Invasive X-ray coronary angiography and non-invasive coronary computed tomography angiography (CCTA) are the gold standard imaging modalities for the assessment of CAD [2–7]. Despite being highly diagnostic, X-ray coronary angiography is limited by invasive complications (e.g., death, stroke, myocardial and vascular injury, pain, and bleeding), whilst both X-ray coronary angiography and CCTA are limited by the risks from ionizing radiation and contrast-mediated nephropathy. There is therefore a clear need for an alternative imaging modality for the early detection and long-term monitoring of CAD, which is free of the risks associated with X-ray coronary angiography and CCTA.

Coronary magnetic resonance angiography

Cardiovascular magnetic resonance (CMR) could be a safe, non-invasive alternative for the imaging of coronary artery stenosis without ionizing radiation or iodinated contrast

[1]*Work in progress. The application is currently under development and is not for sale in the U.S. and in other countries. Its future availability cannot be ensured.*

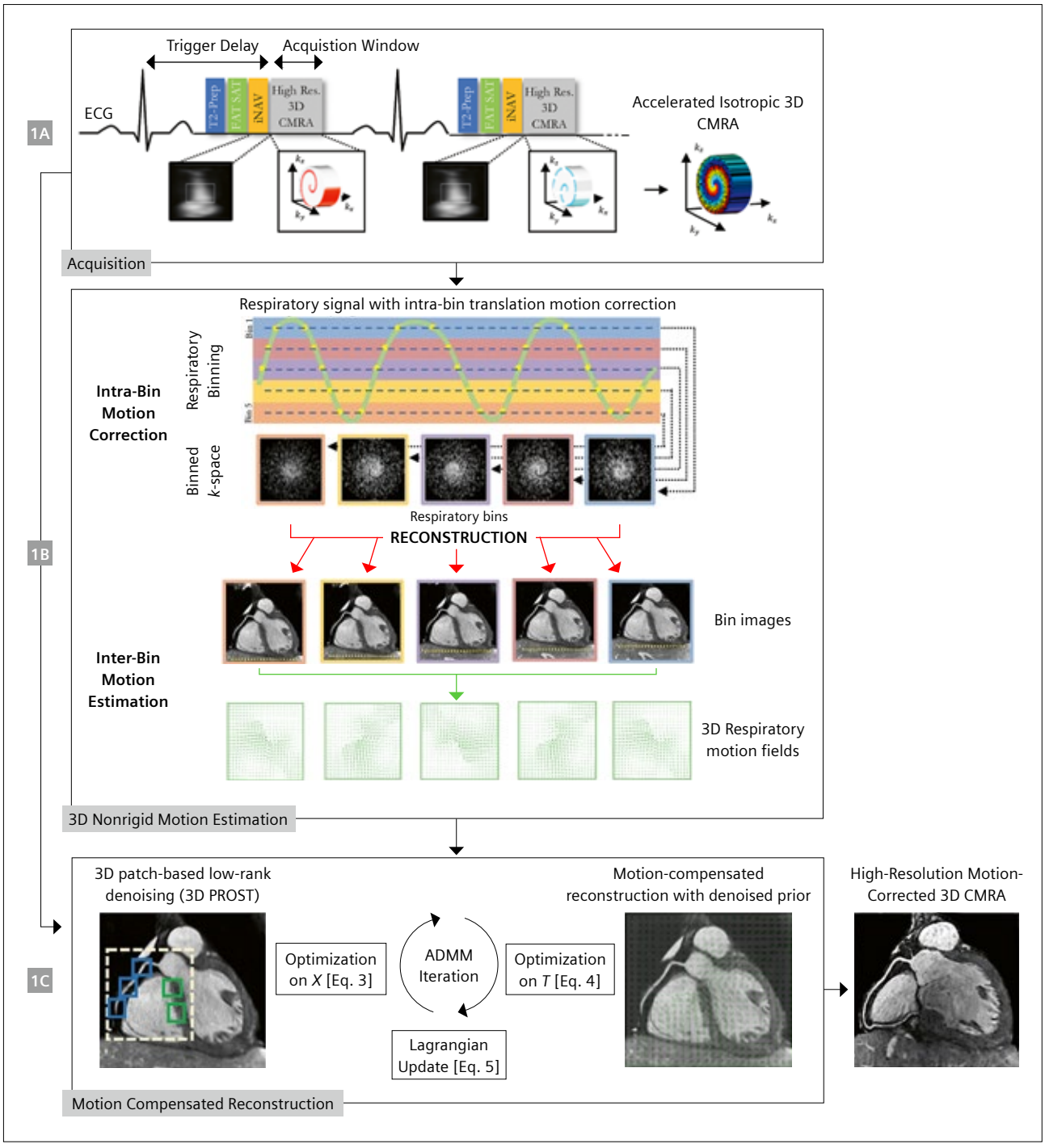

1 Schematic overview of the proposed accelerated free-breathing 3D CMRA acquisition with sub-millimeter isotropic resolution, 100% scan efficiency, and non-rigid motion-compensated PROST reconstruction. **(1A)** CMRA acquisition is performed with an undersampled 3D variable density spiral-like Cartesian trajectory with golden angle between spiral-like interleaves (VD-CASPR), preceded by 2D image navigators (iNAV) to allow for 100% scan efficiency, and beat-to-beat translational respiratory-induced motion correction of the heart. **(1B)** Foot-head respiratory signal is estimated from the 2D iNAVs and used to assign the acquired data to 5 respiratory bins and translation-corrected respiratory bins. Subsequent reconstruction of each bin is performed using soft-gated SENSE, and 3D non-rigid motion fields are then estimated from the 5 reconstructed datasets. **(1C)** The final 3D whole-heart motion-corrected CMRA image is obtained using the proposed 3D patch-based (PROST) non-rigid motion-compensated reconstruction.
Abbreviations: CMRA = coronary magnetic resonance angiography; PROST = patch-based undersampled reconstruction; ADMM = alternating direction method of multipliers.
Adapted and reproduced with permission from Bustin et al. [22].

agent. Large multi-center studies have demonstrated the clinical potential of coronary magnetic resonance angiography (CMRA) against X-ray coronary angiography for the anatomical assessment of CAD with per-patient sensitivity, specificity, and negative predictive value of up 94%, 82%, and 92% respectively [8–10]. However, widespread clinical implementation of CMRA is currently limited to suspected anomalous coronary arteries, suspected coronary artery aneurysms (e.g., Kawasaki's disease), coronary artery graft patency assessment, assessment of the proximal coronary arteries, and patients with renal impairment who are unable to receive iodinated contrast [11–13]. The very limited and specific clinical use of CMRA is due to long and unpredictable acquisition times, cumbersome scan planning, lower spatial resolution (usually 1–2 mm anisotropic), and motion-related (cardiac, respiratory, and patient) degradation of image quality.

In a similar fashion to CCTA, CMRA overcomes cardiac motion artifacts by using prospective electrocardiographic (ECG) gating to acquire data during the quiescent phase of the cardiac cycle when coronary artery motion is minimal [11], usually in mid-to-late diastole. In cases of cardiac arrhythmias and variable heart rates, which disproportionately impact the diastolic phase of the cardiac cycle, systolic imaging is the preferred option [11]. An alternative retrospective ECG gating approach is to continuously acquire data throughout the cardiac cycle and then reconstruct multiple cardiac phases and select the phase with the sharpest images or fewest motion artefacts [14, 15].

To compensate for the respiratory motion artifacts during free-breathing acquisitions, conventional CMRA estimates the respiratory displacement and deformation of the heart and surrounding tissues using the diaphragmatic 1D navigator approach [11, 16–18]. Here the liver-diaphragm interface lends itself for motion tracking, with the increased signal-to-noise ratio (SNR) of the right hemi diaphragm used as a surrogate to track the superior-inferior motion of the heart during the respiratory cycle, and with respiratory gating enabled to obtain image data at the quiescent phase of end of expiration [16, 19, 20, 17]. However, there is a non-linear relationship between the displacement of the diaphragm and the heart, requiring a patient-specific correction factor, which is usually set at 0.6 (population average) when gating is combined with respiratory motion correction [16]. Furthermore, only data within a small (end-expiration) respiratory gating window is accepted, significantly reducing scan efficiency and leading to prolonged and unpredictable acquisition times [21]. Moreover, prospective or retrospective translational motion compensation can only be applied in the superior-inferior direction [21]. Finally, this approach adds complexity as detailed scan planning and defining separate imaging parameters for the navigator acquisition are required, further increasing scan time and costs [16]. In addition, a fully sampled 3D whole-heart CMRA acquisition at high spatial resolution is associated with long acquisition times (up to 30 minutes), regardless of cardiac and respiratory motion gating, which leads to patient discomfort and patient-related motion artifacts.

To overcome these limitations, we have leveraged recent advances in CMR technology including trajectory design, motion correction, and undersampled reconstruction techniques – to propose a novel, highly accelerated, high-spatial-resolution (sub-1 mm^3), free-breathing, non-contrast, 3D whole-heart CMRA framework in a clinically feasible and 100% predictable acquisition time.

Proposed coronary magnetic resonance angiography framework

The proposed CMRA framework was developed on a 1.5T CMR scanner (MAGNETOM Aera, Siemens Healthcare, Erlangen, Germany) with a dedicated 32-channel spine coil and an 18-channel body coil. It combines a highly undersampled variable-density Cartesian acquisition with an image navigator (iNAV) to enable model-free 2D translational and 3D non-rigid motion estimation, and finally deploys a motion-corrected 3D patch-based low-rank image reconstruction (PROST) algorithm[1] to reconstruct the undersampled acquisition. These steps are outlined in more detail in the following sections and in the article by Bustin et al. [22].

Accelerated CMRA acquisition

An undersampled (3- to 4-fold) free-breathing 3D whole-heart, balanced steady-state free-precession (bSSFP) sequence with a 3D variable-density spiral-like Cartesian trajectory (VD-CASPR) with golden-angle step was employed as previously proposed [23] (Fig. 1). A low-resolution 2D iNAV preceded each spiral-like interleave to allow 100% scan efficiency, predictable scan time, and 2D translational motion estimation of the heart on a beat-to-beat basis. The 2D iNAVs were obtained by spatially encoding the startup profiles of the bSSFP sequence [24]. A spectrally selective SPIR (Spectral Presaturation with Inversion Recovery) fat saturation pulse with a constant flip angle (FA) of 130° was used to improve coronary depiction and minimize fat-related aliasing artifacts. An adiabatic T2 preparation pulse [25, 26] was played at each heartbeat in order to enhance the contrast between blood and cardiac muscle and to avoid the use of extracellular contrast agents.

[1] *Work in progress. The application is currently under development and is not for sale in the U.S. and in other countries. Its future availability cannot be ensured.*

Beat-to-beat 2D translational motion estimation
Beat-to-beat 2D translational motion correction was performed as previously proposed in [27, 28]. Briefly, foot-head (FH) and right-left (RL) translational respiratory motion of the heart was extracted from the iNAVs using a template-matching algorithm with normalized cross-correlation as similarity measure [24]. The reference template was manually selected during scan planning on a region encompassing the subject's heart. The FH respiratory signal was used to sort the acquired data into five respiratory states or bins. Intra-bin 2D translational motion estimation was performed by correcting the data for each bin to the same respiratory position (taken as the bin center) (Fig. 1). This correction was implemented by modulating the *k*-space data with a linear phase shift according to the previously estimated respiratory motion [27].

Bin-to-bin non-rigid motion estimation
In this framework, the acquired 3D CMRA data is under-sampled (3- to 4-fold), with the resulting binned *k*-spaces being highly accelerated (~15- to 20-fold). Soft-gating iterative sensitivity encoding reconstruction [27] was employed to reconstruct each respiratory bin. Bin-to-bin 3D non-rigid motion estimation was subsequently performed using spline-based free-form deformation [29], considering the end-expiration bin as reference image (Fig. 1).

3D patch-based non-rigid motion-compensated reconstruction (non-rigid PROST)
Following this step, the estimated 3D non-rigid motion fields are then directly incorporated into a general matrix description reconstruction framework [30, 31]. In contrast to previous CMRA studies where the data are acquired either fully sampled [27] or with modest undersampling factors [28], our proposed high-resolution (0.9 mm^3) CMRA framework exploits higher undersampling factors (3- to 4-fold) to reach approximately 10-minute acquisition time. 3D patch-based low-rank undersampled reconstruction (3D PROST) has been proposed to highly accelerate sub-mm CMRA imaging with translational motion correction only [23]. 3D PROST reconstruction exploits the inherent redundancies of the complex 3D anatomy of the coronary arteries on a local (i.e., within a patch) and non-local (i.e., between similar patches within a neighborhood) basis, through an efficient iterative low-rank decomposition and singular value thresholding. The proposed non-rigid PROST framework combines 3D PROST with the matrix formalism for non-rigid motion correction, and can be formulated as the unconstrained optimization (found at the bottom of the page), where X is the non-rigid motion-corrected 3D CMRA volume (or "motion-free" image), K is the 2D translational motion-corrected k-space data, E is the encoding operator composed of: A_b the sampling matrix for bin b, F the 3D Fourier transform, S_c the coil sensitivities for coil c, U_b the estimated 3D non-rigid motion fields for bin b and N_{bins} the number of respiratory bins. $||.||_F$ and $||.||_*$ denote the Frobenius and nuclear norms respectively, $P_p(.)$ is the patch-selection operator at voxel p. Equation (1) can be efficiently solved by operator-splitting via alternating direction method of multipliers (ADMM).

Results from a single-center clinical study

The proposed CMRA framework was assessed in a cohort of patients with suspected CAD at Guy's and St Thomas' Hospitals, London, UK. The full results of this clinical study are described in the article by Hajhosseiny et al. [32]. In summary, 50 consecutive patients between 35 and 77 years of age who were referred for a clinically indicated CTCA were invited to undergo a CMRA within the proposed framework. In the absence of contraindications, each patient was treated with intravenous metoprolol in 5 mg increments with a maximum dose of 30 mg, aiming for a target heart rate (HR) < 65 bpm in order to maximize the diastolic acquisition window, reduce HR variability and cardiac motion artefacts. All patients were given 800 mg of sublingual glyceryl trinitrate to promote coronary vasodilation. To assess diagnostic performance, significant coronary stenosis was visually defined as luminal narrowing of ≥ 50% in each of the coronary segments using an intention-to-read approach. The image quality of CMRA images (3D whole-heart dataset and individual vessels) was evaluated using the following scale: 0, non-diagnostic; 1, poor (limited coronary vessel visibility or noisy image); 2, average (coronary vessel visible but diagnostic confidence low); 3, good (coronary artery adequately visualized and diagnostic quality image); and 4, excellent (coronary artery clearly depicted).

All CMRA acquisitions were successfully completed in an imaging time of 10.7 ± 1.4 min (range 8.0–13.3 min), with 100% respiratory scan efficiency. All CMRA acquisi-

(1) $$L_{NR\text{-}PROST}(X,T,Y) := \underset{X,T_p,Y}{\operatorname{argmin}} \| EX - K \|_F^2 + \lambda \sum_p \| T_p \|_* + \frac{\mu}{2} \sum_p \| T_p - P_p(X) - \frac{Y_p}{\mu} \|_F^2$$

(2) $$E = \sum_b^{N_{bins}} A_b F S_c U_b$$

tions were performed in diastole with an average acquisition window of 88 ± 8 ms (range 81–111 ms). Mean age was 55 ± 9 years, 33/50 (66%) were male, and 12/50 (24%) had significant CAD on CTCA.

In total, 95% of CMRA segments were deemed diagnostic, while all left main stem segments were diagnostic on CMRA. Furthermore, 97%, 96%, and 87% of right coronary artery, left anterior descending artery, and left circumflex artery segments were diagnostic on CMRA. Finally, 97%, 97%, and 90% of proximal, middle, and distal CMRA segments were of diagnostic quality.

The sensitivity, specificity, positive predictive value, negative predictive value, and diagnostic accuracy of CMRA for detecting significant CAD were as follows:

- per-patient
  100% (95% CI: 76–100%), 74% (95% CI: 58–85%), 55% (95% CI: 35–73%), 100% (95% CI: 88–100%), and 80% (95% CI: 67–89%) respectively;
- per-vessel
  81% (95% CI: 57–93%), 88% (95% CI: 82–93%), 46% (95% CI: 30–64%), 97% (95% CI: 93–99%), and 88% (95% CI: 81–92%) respectively;
- per-segment
  76% (95% CI: 55–89%), 95% (95% CI: 92–97%), 44% (95% CI: 30–60%), 99% (95% CI: 97–99%), and 94% (95% CI: 91–96%) respectively.

Example images from selected patients with suspected CAD are shown in Figures 2–8.

The proposed CMRA framework (without PROST regularization) has been implemented in-line in the scanner software, providing non-rigid motion corrected reconstructions in ~2–5 min (CPU).

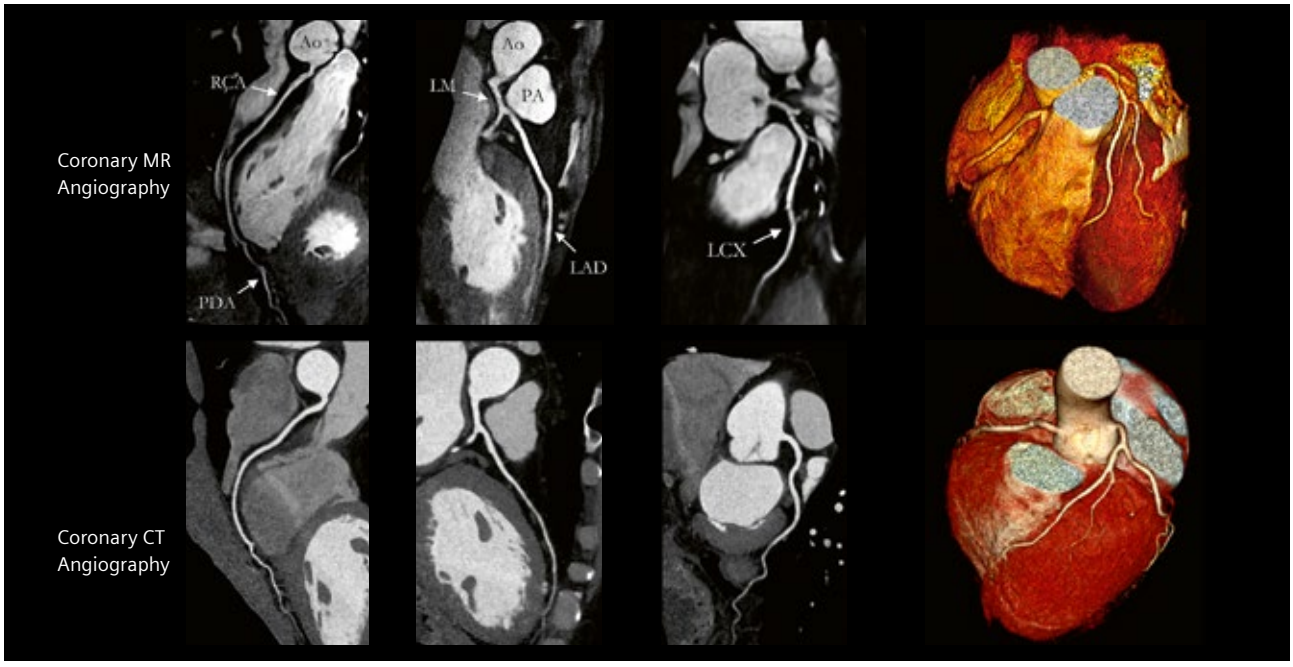

2 Non-contrast whole-heart sub-millimeter isotropic CMRA images of a 53-year-old male patient with normal coronary arteries. Accelerated free-breathing CMRA images acquired and reconstructed with the proposed framework are shown in the top row, revealing the LAD, RCA, and LCX territories. The corresponding reformatted images obtained with contrast-enhanced CCTA are shown in the bottom row. 3D volume-rendered images for both modalities are shown in the right-hand column.
Abbreviations: CMRA = coronary magnetic resonance angiography; CCTA = coronary computed tomography angiography; LAD = left anterior descending artery; RCA = right coronary artery; LCX =left circumflex artery; PDA = posterior descending artery; PA = pulmonary artery; Ao = aorta.
Adapted and reproduced with permission from Bustin et al. [22].

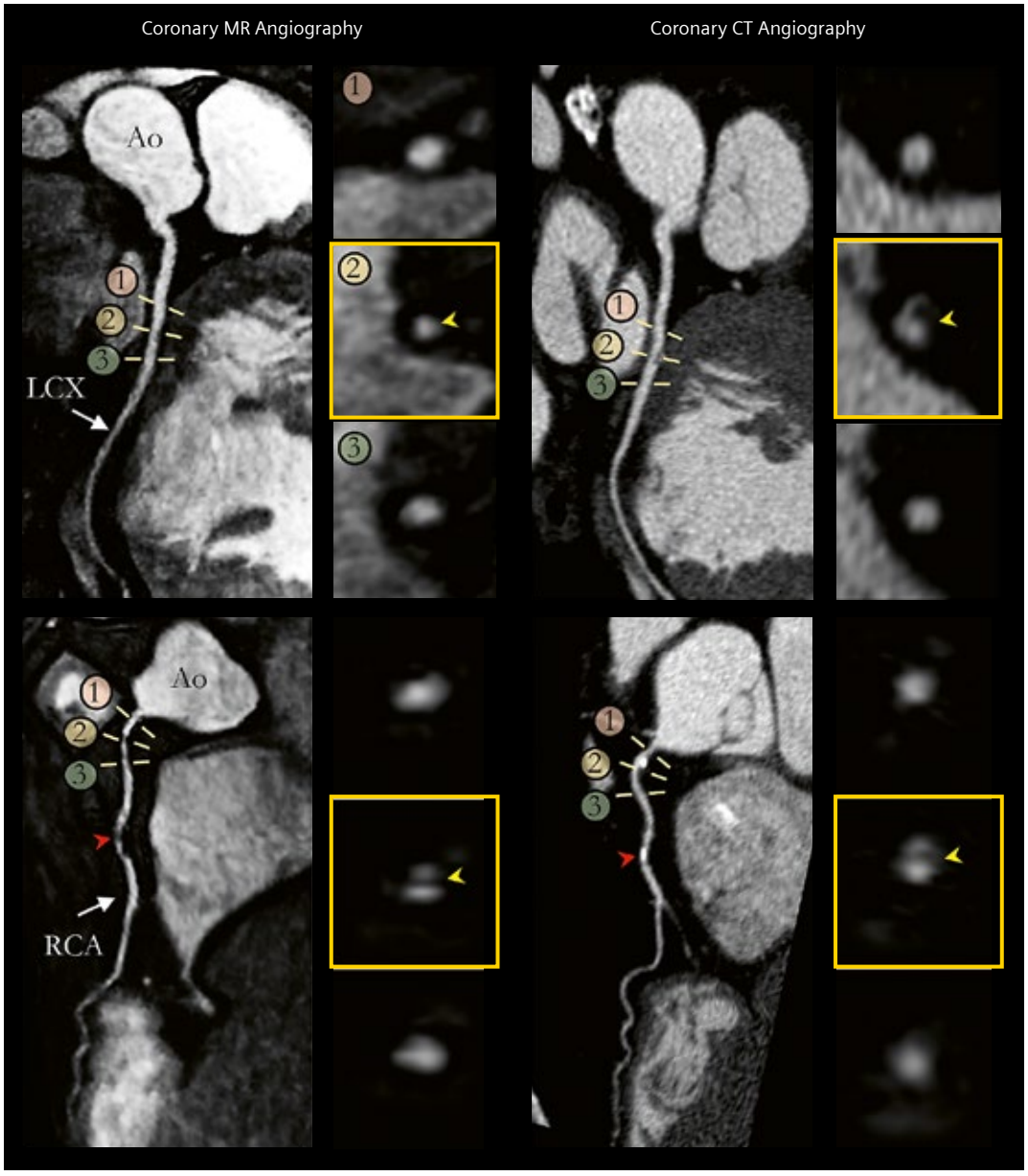

3 Reformatted non-contrast whole-heart sub-millimeter isotropic CMRA (left) and contrast-enhanced CCTA (right) images along the LCX (top) and RCA (bottom) are shown for a 54-year-old male patient. The CCTA images demonstrate mild (< 50%) disease with a calcified plaque within the proximal RCA, severe disease (> 50%) with a partially calcified plaque in the mid-segment of the RCA (red arrows), and mild (< 50%) disease with calcified plaque in the mid-segment of the LCX. Luminal narrowing is seen on the cross-sectional views at the sites of coronary plaque on the CMRA images (yellow arrows).
Abbreviations: CMRA = coronary magnetic resonance angiography; CCTA = coronary computed tomography angiography; LAD = left anterior descending artery; RCA = right coronary artery; LCX = left circumflex artery; Ao = aorta.
Adapted and reproduced with permission from Bustin et al. [22].

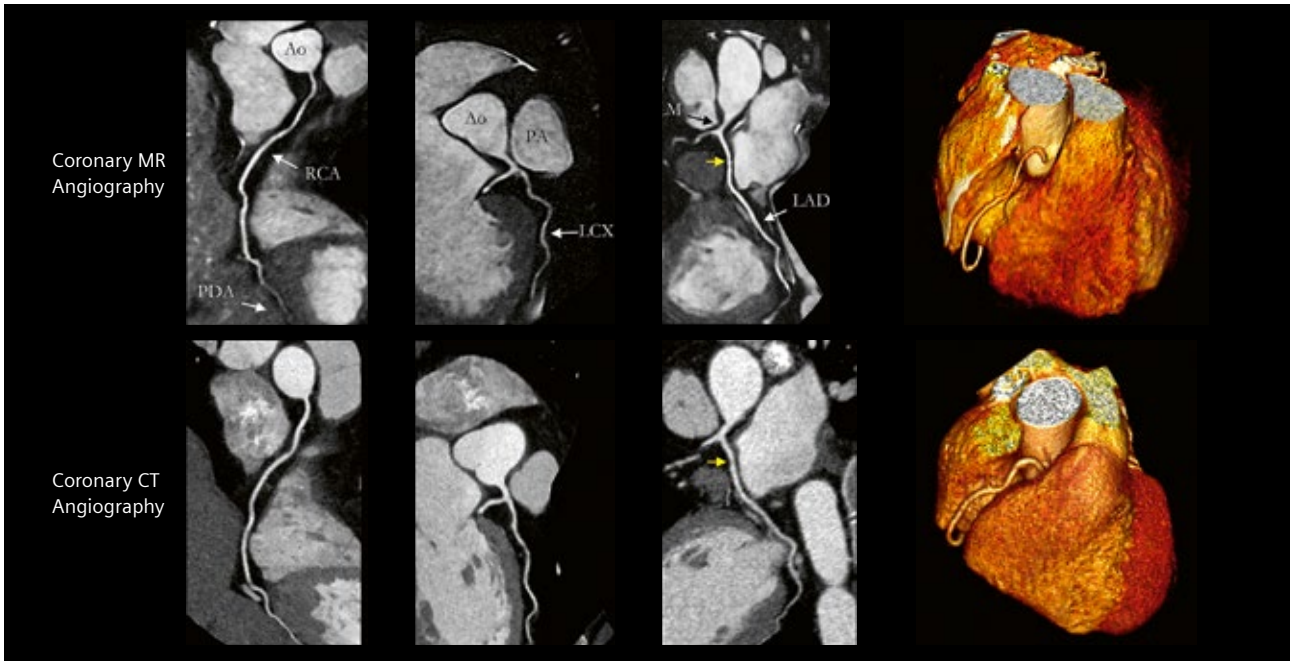

4 Non-contrast whole-heart sub-millimeter isotropic CMRA images of a 35-year-old male patient with normal coronary arteries. The CMRA images acquired and reconstructed with the proposed framework are shown in the top row, revealing the LAD and RCA. The corresponding reformatted images obtained with contrast-enhanced CCTA are shown in the bottom row. The 3D volume-rendered images are shown in the right-hand column, which were both correctly visualized on the CMRA images.
Abbreviations: CMRA = coronary magnetic resonance angiography; CCTA = coronary computed tomography angiography; LAD = left anterior descending artery; RCA = right coronary artery; LCX = left circumflex artery; LM = left main stem; PDA = posterior descending artery; PA = pulmonary artery; Ao = aorta.
Adapted and reproduced with permission from Bustin et al. [22].

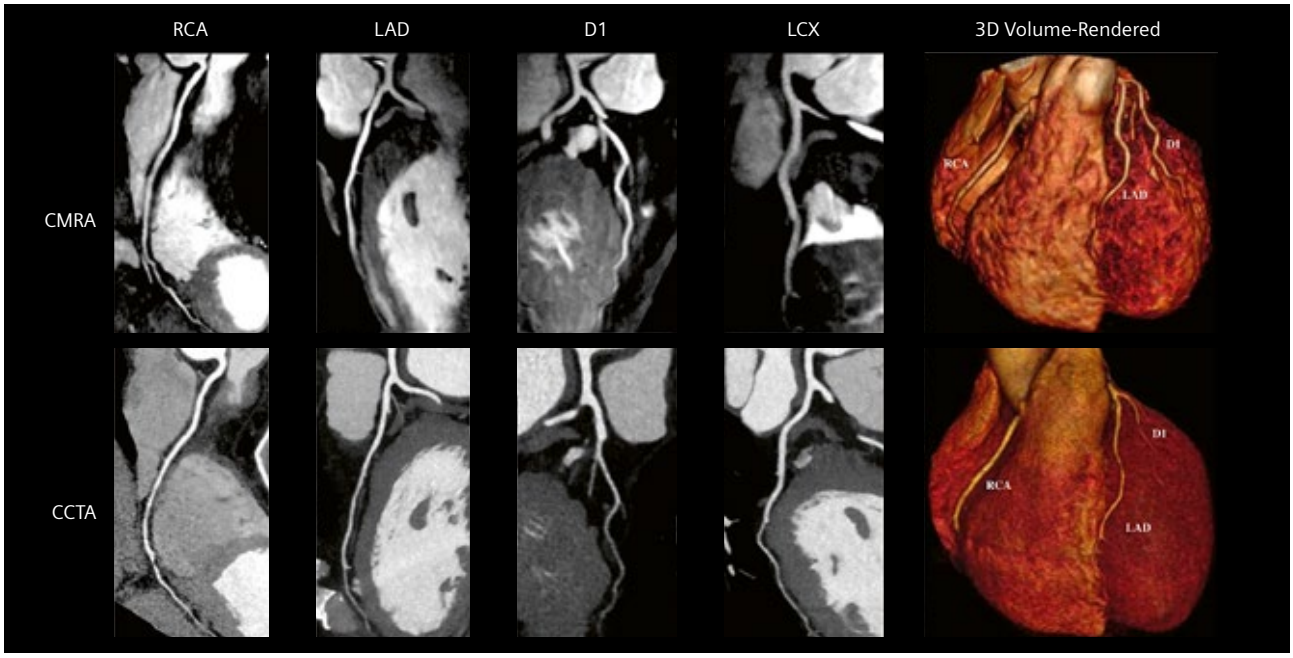

5 Curved multiplanar reformat and 3D volume-rendered non-contrast CMRA and contrast-enhanced CCTA in a 54-year-old male with no significant stenosis.
Abbreviations: CMRA = coronary magnetic resonance angiography; CCTA = coronary computed tomography angiography; RCA = right coronary artery; LAD = left anterior descending artery; D1 = first diagonal artery; LCX = left circumflex artery.
Adapted and reproduced with permission from Hajhosseiny et al. [32].

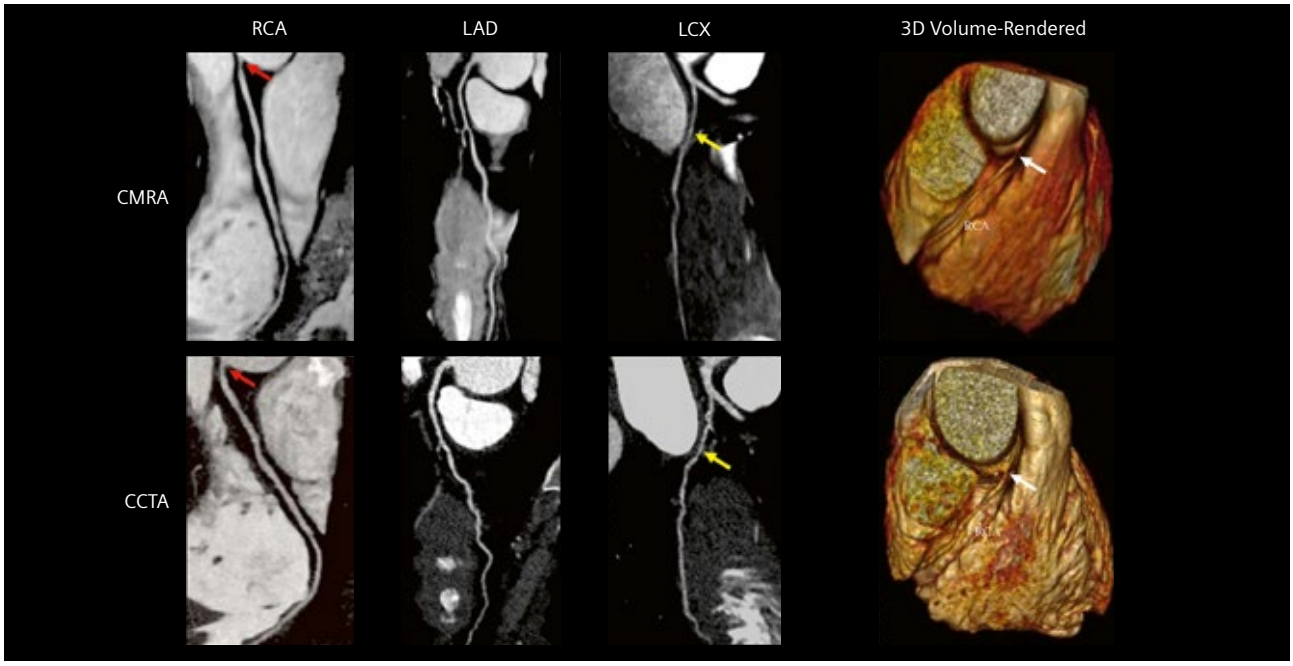

6 Curved multiplanar reformat and 3D volume-rendered non-contrast CMRA and contrast-enhanced CCTA in a 44-year-old male with > 50% non-calcified stenosis in the ostial RCA (red arrows). This can also be seen in the 3D volume-rendered images (white arrows). The yellow arrows represent a > 50% stenosis in the proximal/mid LCX.
Abbreviations: CMRA = coronary magnetic resonance angiography; CCTA = coronary computed tomography angiography; RCA = right coronary artery; LAD = left anterior descending artery; LCX = left circumflex artery.
Adapted and reproduced with permission from Hajhosseiny et al. [32].

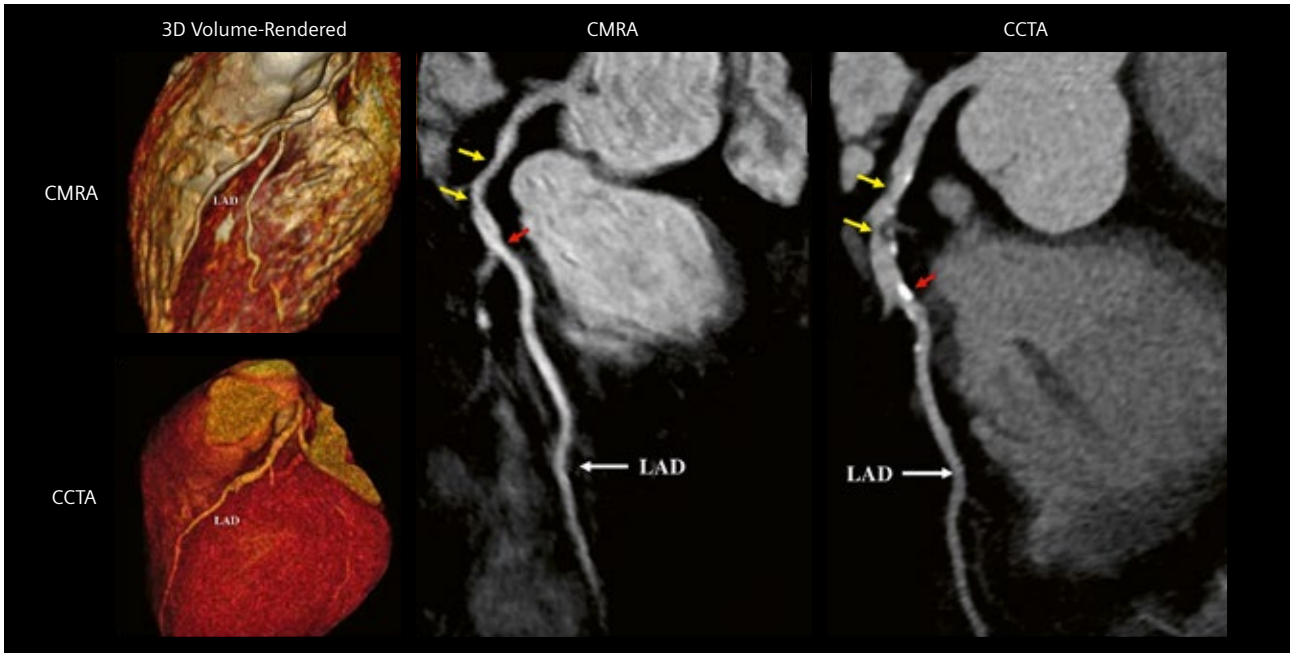

7 Curved multiplanar reformat and 3D volume-rendered non-contrast CMRA and contrast-enhanced CCTA in a 60-year-old male with > 50% partially calcified stenosis in the proximal-to-mid LAD on either side of the first diagonal artery (yellow arrows). The red arrows point to a focal calcified < 50% stenosis just distal to the second diagonal artery.
Abbreviations: CMRA = coronary magnetic resonance angiography; CCTA = coronary computed tomography angiography; LAD = left anterior descending artery. *Adapted and reproduced with permission from Hajhosseiny et al. [32].*

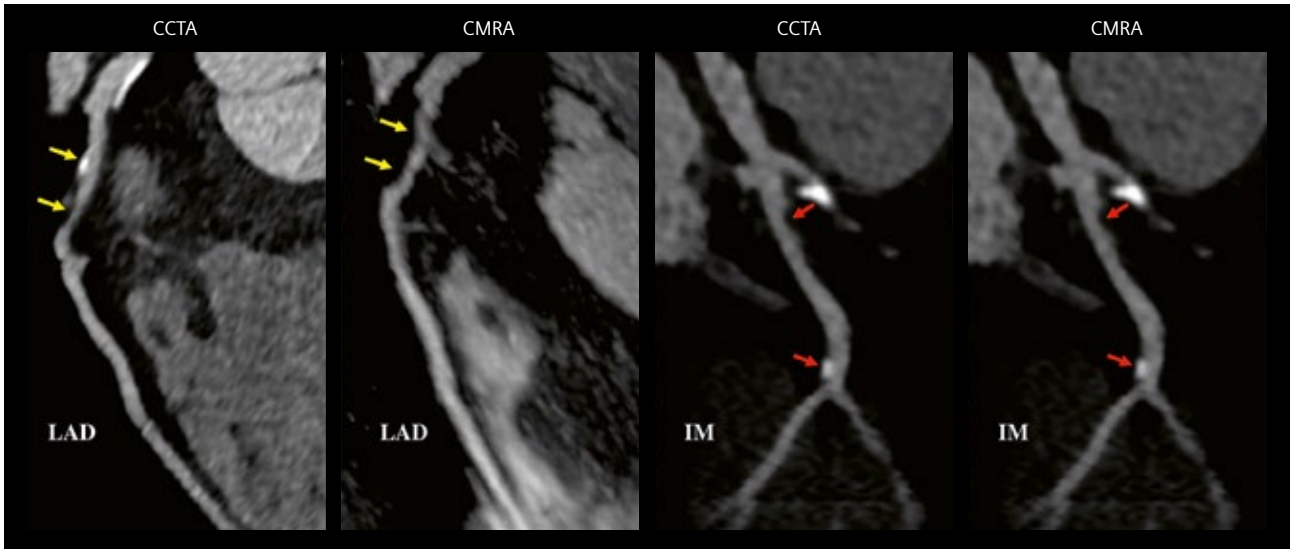

8 Curved multiplanar reformat non-contrast CMRA and contrast-enhanced CCTA in a 57-year-old male with > 50% partially calcified stenosis in the proximal LAD (yellow arrows). The red arrows point to focal < 50% stenosis in the proximal and distal ramus intermedius artery. **Abbreviations:** CMRA = coronary magnetic resonance angiography; CCTA = coronary computed tomography angiography; LAD = left anterior descending artery; IM = ramus intermedius artery. *Adapted and reproduced with permission from Hajhosseiny et al. [32].*

Conclusions

In this initial single-center clinical study, we have introduced a robust, contrast-free, sub-millimeter CMRA framework with predictable and clinically feasible scan times of approximately 10 minutes, achieving highly diagnostic image quality and diagnostic accuracy for excluding significant disease in patients with suspected CAD. This is the first clinical study to assess the diagnostic performance of a 3D contrast-free CMRA approach that enables a predictable scan time of approximately 10 minutes for 0.9 mm^3 spatial-resolution. This was achieved by employing a robust motion corrected free-breathing acquisition with 100% respiratory scan efficiency, using image navigation for 2D translational motion estimation and respiratory data binning combined with 3D non-rigid motion compensated undersampled reconstruction employing a 3- to 4-fold undersampled Cartesian acquisition and a patched-based low-rank reconstruction. Future work will focus on multi-center clinical assessment of this novel framework to determine its clinical applicability in a larger cohort of patients with a wider spectrum of CAD.

References

1 Benjamin EJ, Virani SS, Callaway CW, et al. Heart disease and stroke statistics-2018 update: A report from the American Heart Association. Circulation 2018;137(12):e67–e492. Available at: http://www.ncbi.nlm.nih.gov/pubmed/29386200.

2 Kočka V. The coronary angiography – An old-timer in great shape. Cor Vasa 2015;57(6):e419–e424. Available at: https://www.sciencedirect.com/science/article/pii/S0010865015001009. Accessed August 14, 2018.

3 Tavakol M, Ashraf S, Brener SJ. Risks and complications of coronary angiography: a comprehensive review. Glob J Health Sci. 2012;4(1):65–93. Available at: http://www.ncbi.nlm.nih.gov/pubmed/22980117. Accessed August 14, 2018.

4 Kolossváry M, Szilveszter B, Merkely B, Maurovich-Horvat P. Plaque imaging with CT-a comprehensive review on coronary CT angiography based risk assessment. Cardiovasc Diagn Ther. 2017;7(5):489–506. Available at: http://www.ncbi.nlm.nih.gov/pubmed/29255692. Accessed August 14, 2018.

5 Hamilton M, Baumbach A. Non invasive coronary imaging with computed tomography. [journal on the Internet]. 2007; 5(20). Available at: https://www.escardio.org/Journals/E-Journal-of-Cardiology-Practice/Volume-5/Non-Invasive-Coronary-Imaging-With-Computed-Tomography-Title-Non-Invasive-Cor. Accessed August 14, 2018.

6 Alfakih K, Byrne J, Monaghan M. CT coronary angiography: a paradigm shift for functional imaging tests. Open Hear. 2018;5(1):e000754. Available at: http://www.ncbi.nlm.nih.gov/pubmed/29632679. Accessed August 14, 2018.

7 Doris MK, Newby DE. How should CT coronary angiography be integrated into the management of patients with chest pain and how does this affect outcomes? Eur Heart J - Qual Care Clin. Outcomes 2016;2(2):72–80. Available at: https://academic.oup.com/ehjqcco/article-lookup/doi/10.1093/ehjqcco/qcv027. Accessed August 14, 2018.

8 Kim WY, Danias PG, Stuber M, et al. Coronary magnetic resonance angiography for the detection of coronary stenoses. N Engl J Med. 2001;345(26):1863–1869. Available at: http://www.ncbi.nlm.nih.gov/pubmed/11756576. Accessed July 26, 2019.

9 Yang Q, Li K, Liu X, et al. Contrast-Enhanced Whole-Heart Coronary Magnetic Resonance Angiography at 3.0-T. A Comparative Study With X-ray Angiography in a Single Center. J Am Coll Cardiol. 2009;54(1):69-76.

10 Kato S, Kitagawa K, Ishida N, et al. Assessment of coronary artery disease using magnetic resonance coronary angiography: a national multicenter trial. J Am Coll Cardiol. 2010;56(12):983–91. Available at: http://linkinghub.elsevier.com/retrieve/pii/S0735109710024691. Accessed September 30, 2018.
11 Sriharan M, McParland P, Harden S, Nicol E. Non-Invasive Coronary Angiography. In: Branislav B. Coronary Angiography - Advances in Noninvasive Imaging Approach for Evaluation of Coronary Artery Disease. [book on the Internet]. London: InTech, 2011:99-122. DOI: 10.5772/22475. Available at: http://www.intechopen.com/books/coronary-angiography-advances-in-noninvasive-imaging-approach-for-evaluation-of-coronary-artery-disease/non-invasive-coronary-angiography. Accessed August 16, 2018.
12 Mangla A, Oliveros E, Williams KA, Kalra DK. Cardiac imaging in the diagnosis of coronary artery disease. Curr Probl Cardiol. 2017;42(10):316–366. Available at: https://www.sciencedirect.com/science/article/pii/S0146280617300725?via%3Dihub#bib116. Accessed August 16, 2018.
13 Hamdy A, Ishida M, Sakuma H. Cardiac MR assessment of coronary arteries. CVIA 2017;1(1):49–59. Available at: https://doi.org/10.22468/cvia.2016.00066. Accessed December 11, 2018.
14 Coppo S, Piccini D, Bonanno G, et al. Free-running 4D whole-heart self-navigated golden angle MRI: Initial results. Magn Reson Med. 2015;74(5):1306–1316. Available at: http://www.ncbi.nlm.nih.gov/pubmed/25376772. Accessed September 3, 2018.
15 Pang J, Bhat H, Sharif B, et al. Whole-heart coronary MRA with 100% respiratory gating efficiency: Self-navigated three-dimensional retrospective image-based motion correction (TRIM). Magn Reson Med. 2014;71(1):67–74. Available at: http://doi.wiley.com/10.1002/mrm.24628. Accessed August 18, 2018.
16 Henningsson M, Botnar RM. Advanced respiratory motion compensation for coronary MR angiography. Sensors (Basel). 2013;13(6):6882–99. Available at: http://www.ncbi.nlm.nih.gov/pubmed/23708271. Accessed August 17, 2018.
17 Ehman RL, Felmlee JP. Adaptive technique for high-definition MR imaging of moving structures. Radiology 1989;173(1):255–263. Available at: http://www.ncbi.nlm.nih.gov/pubmed/2781017. Accessed August 17, 2018.
18 McConnell M V, Khasgiwala VC, Savord BJ, et al. Comparison of respiratory suppression methods and navigator locations for MR coronary angiography. AJR Am J Roentgenol. 1997;168(5):1369–1375. Available at: http://www.ncbi.nlm.nih.gov/pubmed/9129447. Accessed August 17, 2018.
19 Danias PG, McConnell M V, Khasgiwala VC, Chuang ML, Edelman RR, Manning WJ. Prospective navigator correction of image position for coronary MR angiography. Radiology. 1997;203(3):733–736. Available at: http://www.ncbi.nlm.nih.gov/pubmed/9169696. Accessed August 17, 2018.
20 Nehrke K, Börnert P, Groen J, Smink J, Böck JC. On the performance and accuracy of 2D navigator pulses. Magn Reson Imaging 1999;17(8):1173–81. Available at: http://www.ncbi.nlm.nih.gov/pubmed/10499679. Accessed August 17, 2018.
21 Correia T, Ginami G, Cruz G, et al. Optimized respiratory-resolved motion-compensated 3D Cartesian coronary MR angiography. Magn Reson Med. 2018;80(6):2618–2629. Available at: http://www.ncbi.nlm.nih.gov/pubmed/29682783. Accessed August 17, 2018.
22 Bustin A, Rashid I, Cruz G, et al. 3D whole-heart isotropic sub-millimeter resolution coronary magnetic resonance angiography with non-rigid motion-compensated PROST. J Cardiovasc Magn Reson. 2020;22(1):https://doi.org/10.1186/s12968-020-00611-5.
23 Bustin A, Ginami G, Cruz G, et al. Five-minute whole-heart coronary MRA with sub-millimeter isotropic resolution, 100% respiratory scan efficiency, and 3D-PROST reconstruction. Magn Reson Med. 2019;81(1):102–115.
24 Henningsson M, Koken P, Stehning C, Razavi R, Prieto C, Botnar RM. Whole-heart coronary MR angiography with 2D self-navigated image reconstruction. Magn Reson Med. 2012;67(2):437–445. Available at: http://www.ncbi.nlm.nih.gov/pubmed/21656563. Accessed August 17, 2018.
25 Nezafat R, Stuber M, Ouwerkerk R, Gharib AM, Desai MY, Pettigrew RI. B1-insensitive T2 preparation for improved coronary magnetic resonance angiography at 3T. Magn Reson Med. 2006;55(4):858–64.
26 Botnar RM, Stuber M, Danias PG, Kissinger K V, Manning WJ. Improved coronary artery definition with T2-weighted, free-breathing, three-dimensional coronary MRA. Circulation. 1999;99(24):3139–3148.
27 Cruz G, Atkinson D, Henningsson M, Botnar RM, Prieto C. Highly efficient nonrigid motion-corrected 3D whole-heart coronary vessel wall imaging. Magn Reson Med. 2017;77(5):1894–1908. Available at: http://doi.wiley.com/10.1002/mrm.26274. Accessed August 20, 2018.
28 Correia T, Cruz G, Schneider T, Botnar RM, Prieto C. Technical note: Accelerated nonrigid motion-compensated isotropic 3D coronary MR angiography. Med Phys. 2018;45(1):214–222.
29 Rueckert D, Sonoda LI, Hayes C, Hill DL, Leach MO, Hawkes DJ. Nonrigid registration using free-form deformations: application to breast MR images. IEEE Trans Med Imaging. 1999;18(8):712–721.
30 Batchelor PG, Atkinson D, Irarrazaval P, Hill DLG, Hajnal J, Larkman D. Matrix description of general motion correction applied to multishot images. Magn Reson Med. 2005;54(5):1273–1280.
31 Cruz G, Atkinson D, Buerger C, Schaeffter T, Prieto C. Accelerated motion corrected three-dimensional abdominal MRI using total variation regularized SENSE reconstruction. Magn Reson Med. 2016;75(4):1484–1498.
32 Hajhosseiny R, Rashid I, Bustin A, Munoz C, Cruz G, Nazir M.S, Grigoryan K, Ismail T.F, Preston R, Neji R, Kunze K, Razavi R, Chiribiri A, Masci P.G, Rajani R, Prieto C, Botnar R.M. Clinical comparison of sub-mm high-resolution non-contrast coronary MRA against coronary CTA in patients with low-intermediate risk of CAD: A single center trial. J Cardiovasc Magn Reson. 2021; IN PRESS.

Contact

Reza Hajhosseiny, M.D.
School of Biomedical Engineering and Imaging Sciences
King's College London
3rd floor Lambeth Wing
London, SE1 7EH
United Kingdom
Phone: +44 020 7188 7188
reza.hajhosseiny@kcl.ac.uk
Twitter: @KCL_CardiacMR

Infrared Thermally Enhanced 3D TOF MOTSA MR Angiography for Visualizing the Arteries of the Face

Marc Mespreuve, M.D., Ph.D.[1]; Karl Waked, M.D.[2]; Yannick De Brucker, M.D.[3]; Greta Vandemaele, Ph.D.[4]; Benoit Hendrickx, M.D., Ph.D.[5]

[1]Department of Medical Imaging, University Hospital Ghent; AZ St Maarten, Mechelen, Belgium
[2]Department of Plastic and Reconstructive Surgery, University Hospital Brussels, Belgium
[3]Department of Medical Imaging, University Hospital Brussels, Belgium
[4]Siemens Healthineers, MR Applications, Huizingen, Belgium
[5]University Hospital Brussels, and AZ Zeno, Knokke-Heist, Belgium

Three-dimensional time-of-flight magnetic resonance angiography and its limitations

Time-of-flight (TOF) magnetic resonance angiography (MRA) is one of the most important methods of non-contrast neurovascular MRA. TOF MRA is based on the principle of flow-related enhancement. Stationary tissues in an imaged volume become magnetically saturated by multiple repetitive radiofrequency (RF) pulses that reduce their steady-state magnetization levels. Fresh blood flowing into the imaged volume has not experienced these pulses and still has a high initial magnetization. The signal from the inflowing blood appears bright compared to the background tissue. A maximum intensity projection (MIP) technique is then used to create an MR angiogram.

The 3D TOF angiography method is based on a 3D gradient echo (GRE) sequence. Often, a pre-saturation pulse is applied above or below the imaged volume to reduce the signals from venous inflow. Flip angles of 30°–60° are used to maximize the contrast between stationary tissues and blood. Short TE values (< 7 ms) are applied to minimize signal losses from phase dispersion. A maximal enhancement of the blood flow is observed when the vessel is perpendicular to the plane of imaging (in-plane flow is not visible) and has a larger diameter and a high flow. Various modifications of the TOF technique have been developed to reduce in-plane saturation effects and improve visualization of smaller vessels and slow flow. These modifications include the use of variable flip angles, fat suppression, magnetization transfer saturation pulses, and multiple overlapping thin slab acquisition (MOTSA).

3D TOF MOTSA sequence 1.5T	
TR (repetition time)	30 ms
TE (echo time)	6.8 ms
Number of slices per slab (% slice OS)	40 (20% OS)
FOV	180 × 180 mm^2
Flip angle	30 °
Matrix (% phase resolution)	241 × 256 (94%) pixels
Slice thickness (% slice resolution)	0.5 (50%) mm
Averages	2
Acceleration	GRAPPA2
Voxel size acquired	0.7 × 0.7 × 1.0 mm^3
Voxel size reconstructed	0.35 × 0.35 × 0.5 mm^3
Acquisition time	16:14 min

Table 1: MAGNETOM Aera XQ
3D TOF MOTSA sequence 1.5T
Gradient echo sequence with five overlapping slabs (-17.5%).

The principle of combining infrared heat-induced enhancement with a 3D TOF MRA sequence, either with or without compressed sensing

The vascular anatomy of the face is extremely variable. Not only is the arterial course very tortuous, but the localization and depth of the facial arteries and their branches also varies significantly from person to person and even between each side of the face [1–3]. Hence, an ideal plane for the optimal inflow for the different facial arteries is always a compromise. Moreover, many of the vessels are small and have a slow flow.

Previous studies have described heating the face using an infrared (IR) lamp to enlarge the diameter of the vessels and accelerate the flow [4–6].

Recently, the use of compressed sensing (CS) has offered synergistic enhancement for parallel imaging with

sparse sampling and iterative reconstruction. CS speeds up data acquisition with sparse data subsampling. Applying CS reconstruction to the raw data can achieve enhanced image quality. The acceleration makes it possible to significantly reduce the acquisition time, which is especially important for 1.5T MRA, as it involves quite long acquisition times. Compressed sensing applications have been demonstrated for the brain, where it has proven to be very useful in certain exams with lengthy scan times. TOF MRA is a lengthy scan technique, for which the application of compressed sensing has been demonstrated to almost halve scan time while still providing almost equivalent diagnostic information [7].

Technology

The patient is positioned with closed eyes in front of an infrared (IR) light source (300 W) with an InfraCare (Philips, Amsterdam, The Netherlands) screen (which filters out the UV light), at a distance of 30 cm and with their face parallel to the lamp for 15 minutes. The heat induces vasodilatation and enhances the vascular flow, both of which help to improve image acquisition [4–6]. At the same time, the patient is also asked to stimulate their facial muscles by slowly moving their lips and forehead and switching between several facial expressions during the exposure time. This is to further enhance the visualization of the facial arteries by vascular dilatation and increased flow speed [8]. Immediately following IR exposure, the patient is transferred to the MRI unit.

After acquisition of the scout views, a 3D TOF MOTSA MRA sequence is acquired in an oblique coronal plane (tilting of 25° backwards in relation to the line between the glabella and the chin). The initial MRA protocol for a MAGNETOM Aera 1.5T scanner from Siemens Healthcare (with Numaris 4, software version *syngo* MR E11E) is summarized in Table 1 and was developed, based on a previously published study that discusses the MRA sequence in more detail [4]. Table 2 contains the data for a MAGNETOM Sola Fit 1.5T scanner from Siemens Healthcare (NumX *syngo* MR A20) with CS, and Table 3 contains the data for a MAGNETOM Vida 3T scanner from Siemens Healthcare (NumX *syngo* MR A20). During the examination, the patient is asked to remain completely still (this includes their eyes, lips, chin, and cheeks) with their eyes and mouth closed (without pressure on the lips), and their face parallel to the examination table. A multislab MOTSA technique is used to reduce the saturation effect of the signal from the inflowing blood.

Implementation and results

Various previous studies have proven the good results of this technique [4–6]. It is also currently in clinical use at several 3T MRI centers in Europe.

3D TOF MOTSA sequence 1.5T	
TR (repetition time)	26.3 ms
TE (echo time)	5.7 ms
Number of slices per slab (% slice OS)	44 (18% OS)
FOV	180 × 180 mm^2
Flip angle	20 °
Matrix (% phase resolution)	241 × 256 (94%) pixels
Slice thickness (% slice resolution)	0.5 (50%) mm
Averages	2
Acceleration	CS5
Voxel size acquired	0.75 × 0.7 × 0.94 mm^3
Voxel size reconstructed	0.47 × 0.47 × 0.47 mm^3
Interpolation	1.5
Acquisition time	11:35 min

Table 2: MAGNETOM Sola Fit XQ with Compressed Sensing
3D TOF MOTSA sequence 1.5T
Gradient echo sequence with seven overlapping slabs (-30%).

3D TOF MOTSA sequence 3T	
TR (repetition time)	30 ms
TE (echo time)	4.92 ms
Number of slices per slab (% slice OS)	40 (20% OS)
FOV	180 × 180 mm^2
Flip angle	30 °
Matrix (% phase resolution)	241 × 256 (94%) pixels
Slice thickness (% slice resolution)	0.5 (50%) mm
Averages	1
Acceleration	GRAPPA2
Voxel size acquired	0.8 × 0.8 × 1.0 mm^3
Voxel size reconstructed	0.4 × 0.4 × 0.5 mm^3
Interpolation	2
Acquisition time	9:21 min

Table 3: MAGNETOM Vida
3D TOF MOTSA sequence 3T
Gradient echo sequence with seven overlapping slabs (-18%).

In the first series, all 3D TOF MOTSA MRA images were acquired on a 1.5T full-body MR system (MAGNETOM Aera, Siemens Healthcare, Erlangen, Germany), using a dedicated 20-channel head coil. Additionally, a flexible wrap-around 4-channel surface coil was mounted on top of the head coil (Fig. 1) [4]. Figure 2 shows a comparison of a 3D TOF MOTSA MRA without (A) and with (B) previous IR exposure.

In order to reduce the examination time and obtain a stronger signal, further series with 3T MRI were added [6]. However, as more than 60% of all MR scanners globally are 1.5 Tesla machines, there is a need for an optimal 1.5T sequence and especially for a reduction in the examination time.

Figure 3 shows the same volunteer examined using a 1.5T MAGNETOM scanner with and without Compressed Sensing (MAGNETOM Aera and MAGNETOM Sola Fit, Siemens Healthcare, Erlangen, Germany), and using a 3T scanner (MAGNETOM Vida, Siemens Healthcare, Erlangen, Germany) in order to compare the individual results. The acquisition time was 9 minutes and 21 seconds for the 3T,

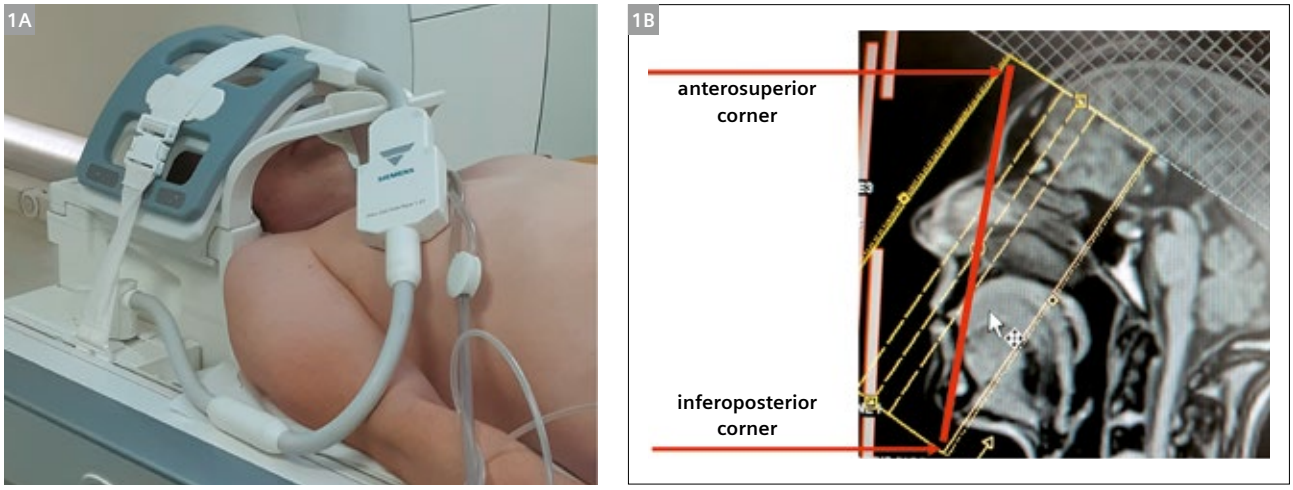

1 **Position of the head coil and the flex coil for the MRA (1A), and position of the 3D TOF MOTSA slab block on the localizer (1B)**
(1A) Flexible wrap-around 4-channel surface coil can be mounted on top of the head coil to increase signal reception from the facial arteries. **(1B)** The line drawn from the glabella to the chin transects the slab position block from the anterosuperior corner to the inferoposterior corner. A magnetic saturation slab is positioned above the slab block.

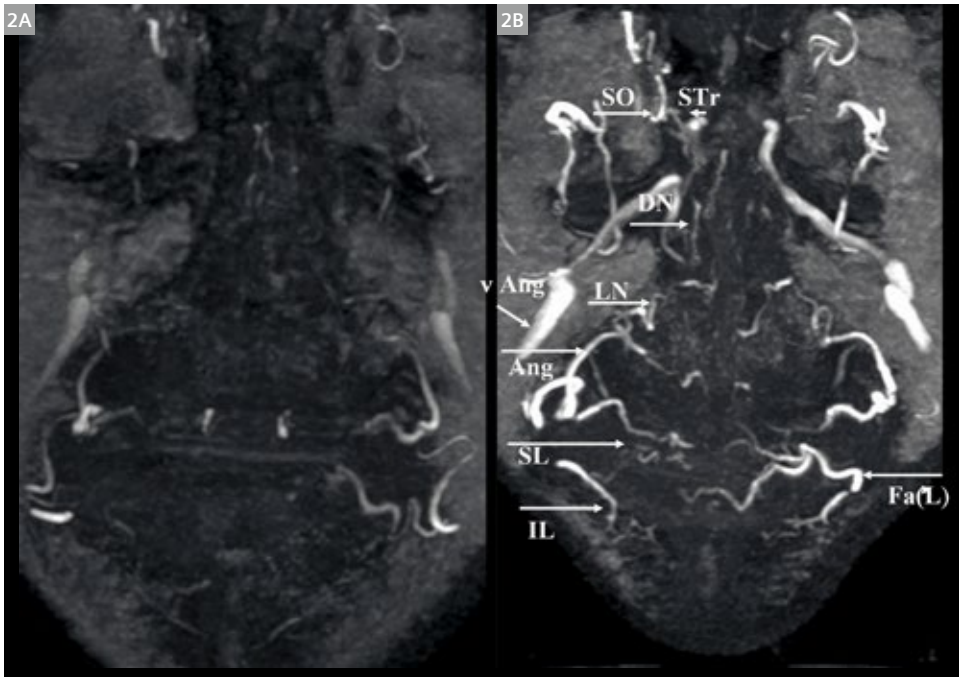

2 **MRA findings (MIP of 3D TOF MOTSA) without (2A) and with (2B) previous IR exposure**
The IR exposure results in a far better visualization of all facial vessels, with a larger caliber of the arteries and a higher visual signal. Superior (SL) and inferior labial artery (IL), angular artery (Ang), lateral nasal artery (LN), dorsal nasal artery (DN), supratrochlear artery (STr), supraorbital artery (SO), facial artery (Fa), and angular vein (vAng).

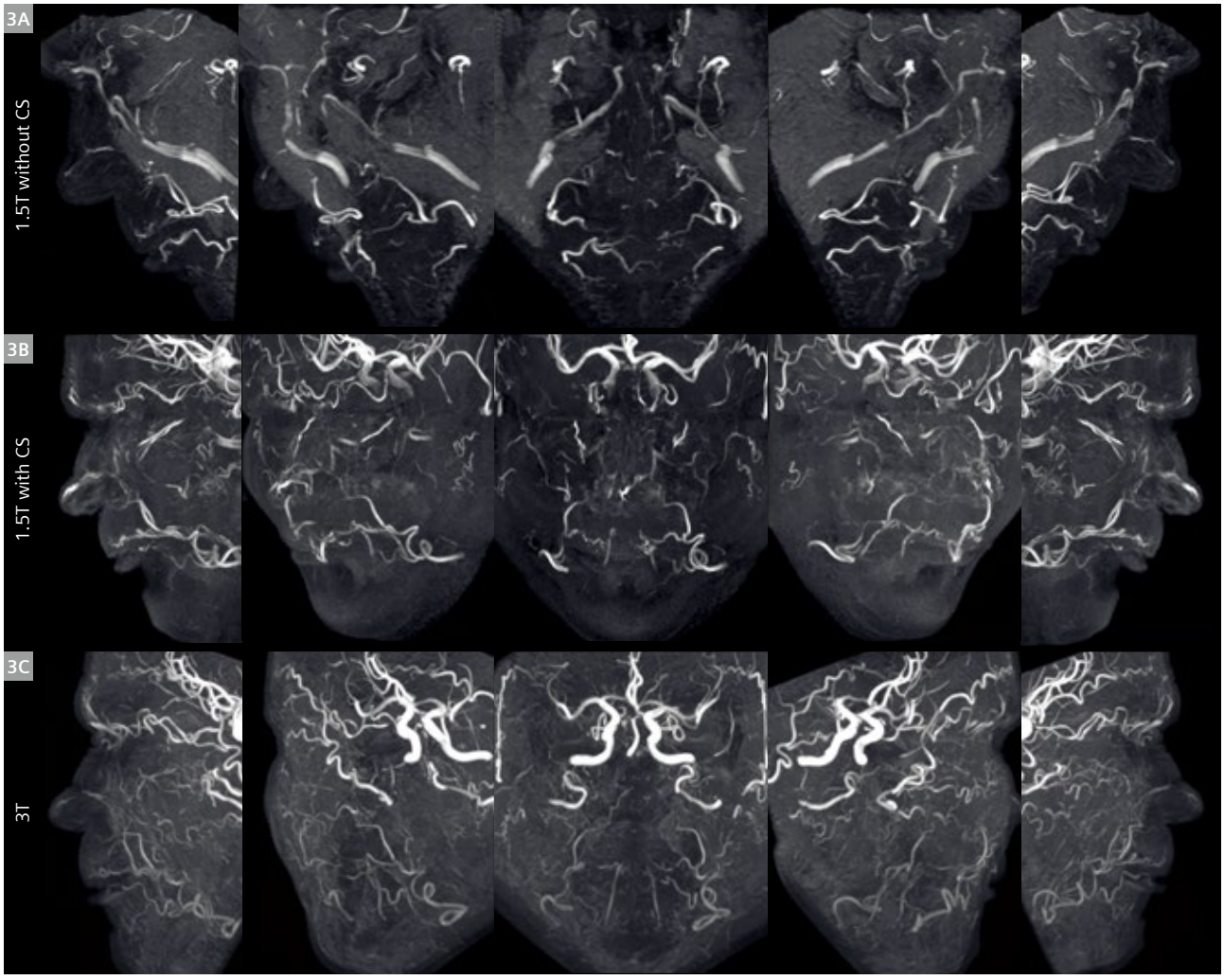

3 **MRA findings (MIP of 3D TOF MOTSA)**
(3A) 1.5T without Compressed Sensing; **(3B)** 1.5T with Compressed Sensing; **(3C)** 3T.

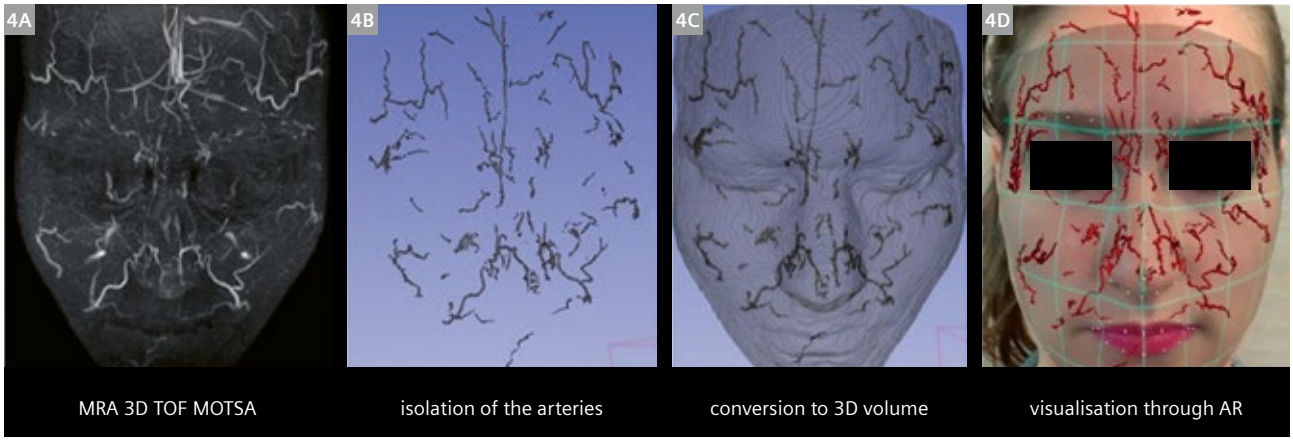

4 **MRA findings and data processing cycle in a 26-year-old female**
(4A) Frontal view of an MIP from the 3D TOF MOTSA.
(4B) Image after isolation of the arteries.
(4C) Conversion to a 3D volume using the MRI data (rotated MIP over 180° from right to left and native image DICOM data).
(4D) Visualization using augmented reality (AR) and projection onto the patient's face with a smartphone camera.

16 minutes and 14 seconds for the 1.5T, and 11 minutes and 35 seconds for the 1.5T with CS (two averages). This illustrates the acceptability of 1.5T MRI examinations compared to 3T, and indicates that they are ready for general use.

Afterwards, the native DICOM images and the MIPs are processed by an experimental 3D software program which isolates the superficial subcutaneous arteries and creates a 3D volume. Using augmented reality, these patient-specific arterial 3D volumes are visualized and projected onto the patient's face (Fig. 4) with a smartphone.

Conclusion

Our experience shows that combining IR heat enhancement and a 3D TOF MRA sequence makes it feasible to visualize a large number of facial arteries in a radiation-free, contrast-free, and non-invasive way.

This thermally enhanced 3D TOF MRA imaging technique may provide a solution for acquiring much-needed information about the patient's individual anatomy in order to better plan and execute aesthetic and reconstructive procedures in the face, such as filler injections [6].

Using CS on a 1.5T MRI scanner significantly reduces the examination time to a more acceptable duration, meaning that the many 1.5T MRI systems in use worldwide could potentially be used for the purpose described above.

Contact

Prof. Dr. Marc Mespreuve
Department of Medical Imaging
University Hospital Ghent
Corneel Heymanslaan 10
9000 Ghent
Belgium
and
A.Z. St. Maarten
Liersesteenweg 435
2800 Mechelen
Belgium
marc.mespreuve@skynet.be

References

1 Loukas M, Hullett J, Louis RG Jr, Kapos T, Knight J, Nagy R, et al. A detailed observation of variations of the facial artery, with emphasis on the superior labial artery. Surg Radiol Anat. 2006;28(3):316–24.
2 Cotofana S, Lachman N. Arteries of the Face and Their Relevance for Minimally Invasive Facial Procedures: An Anatomical Review. Plast Reconstr Surg. 2019;143(2):416–426.
3 Tansatit T, Apinuntrum P, Phetudom T. Periorbital and Intraorbital Studies of the Terminal Branches of the Ophthalmic Artery for Periorbital and Glabellar Filler Placements. Aesthetic Plast Surg. 2017;41(3):678–688.
4 Hendrickx B, Waked K, Mespreuve M. Infrared Thermally Enhanced 3-Dimensional Time of Flight Magnetic Resonance Angiography Imaging for the Visualization of the Arteries of the Face. Aesthet Surg J Open Forum. 2020;2(2):ojaa020.
5 Mespreuve M , Waked K, Hendrickx B. Visualization techniques of the facial arteries, J. Cosmet Dermatol. 2021;20(2):386–390. Epub 2020 May 27.
6 Mespreuve M, Waked K, Collard B, De Ranter J, Vanneste F, Hendrickx B. The Usefulness of Magnetic Resonance Angiography to Analyze the Variable Arterial Facial Anatomy in an Effort to Reduce Filler-Associated Blindness: Anatomical Study and Visualization Through an Augmented Reality Application. Aesthet Surg J Open Forum. 2021;3(3):ojab018.
7 Runge V, Heverhagen J. Important Updates for Advanced Imaging Topics, with a Perspective on Improved Patient Throughput. MAGNEOTM Flash. 2021;78:15–21.
8 Hotta K, Behnke BJ, Arjmandi B, Ghosh P, Chen B, Brooks R, et al. Daily muscle stretching enhances blood flow, endothelial function, capillarity, vascular volume and connectivity in aged skeletal muscle. J Physiol. 2018;596(10):1903–1917.

The DICOM files of the figures in this article are available for download at

https://www.magnetomworld.siemens-healthineers.com/clinical-corner/protocols/dicom-images/3d-tof-motsa-mr

- Phoenix is a unique *syngo* tool that allows you to click on an image, drag it into the measurement queue, and instantly duplicate the extracted protocol – TR, TE, bandwidth, number of slices, echo spacing, etc.
- Phoenix ensures reproducibility, e.g., for patient follow-up.
- Phoenix shares optimized protocols on the different MAGNETOM systems you work with.
- Phoenix supports multicenter protocol standardization.

You'll find DICOM images from various systems and all aspects of MRI at
https://www.magnetomworld.siemens-healthineers.com/clinical-corner/protocols/dicom-images

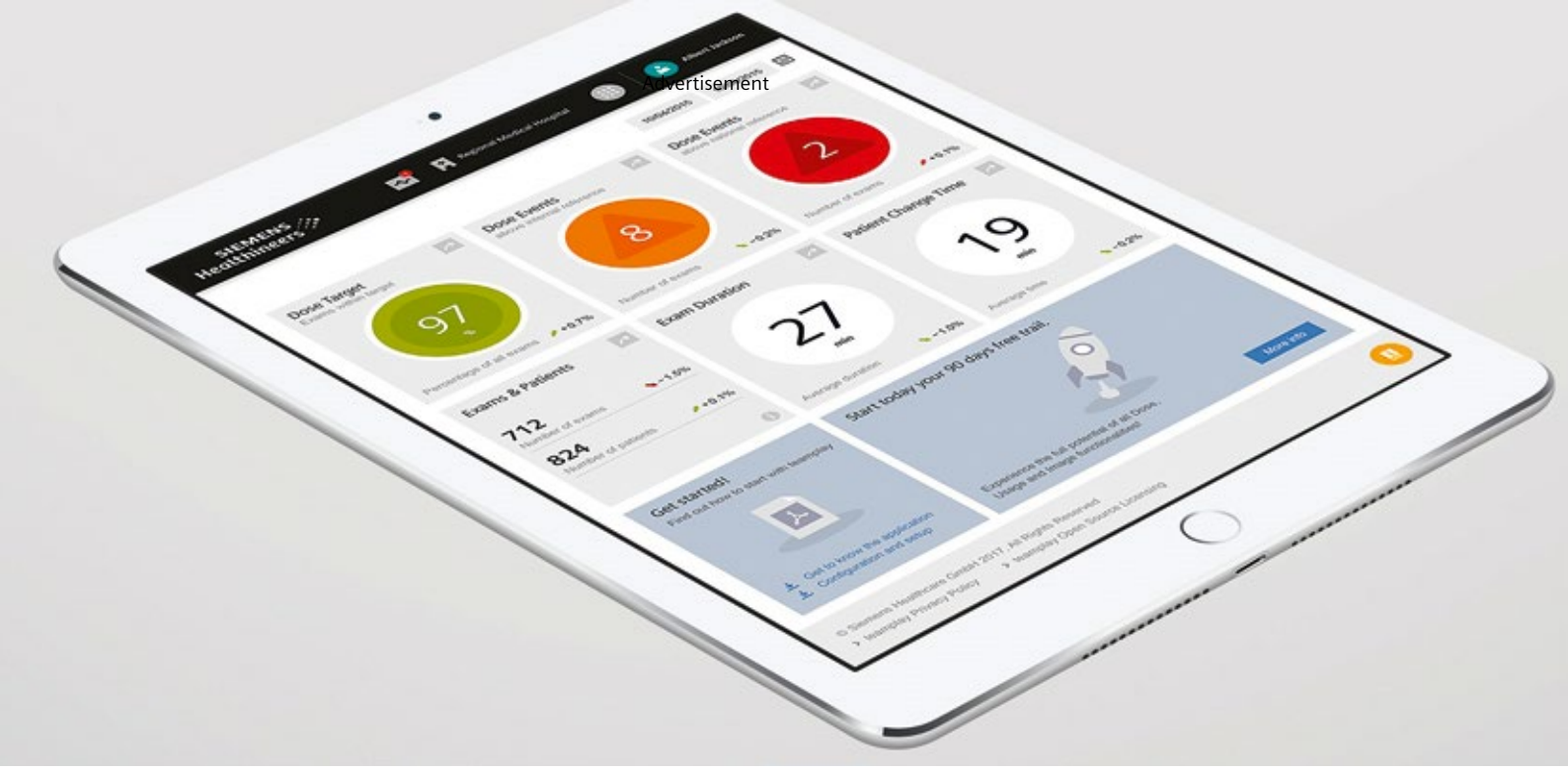

teamplay – Get the most out of your data in radiology and cardiology

healthcare.siemens.de/healthineers-digital-ecosystem/teamplay

To advance digitalization in healthcare, teamplay[1] is a departmental performance management solution that brings together healthcare professionals in a team effort. By connecting medical institutions and their imaging devices, teamplay apps aspire to create the biggest radiology and cardiology team in the world and provide its members with tools to tackle big data and the challenges of increasing cost pressure.

The cloud-based solution teamplay with its apps will help you make prompt and well-informed decisions by offering an intelligible overview of your performance data.

It monitors quantities such as imaging throughput or dose levels, utilization of staff, rooms and resources of your whole department down to every device and procedure, simplifying your reporting and showing you where workflows need adjustments. It links you to other users of teamplay and their data to offer comparable benchmarks[2] and an effortless exchange of images and reports with other healthcare providers.

---

[1] *Please check if teamplay is available in your country.*
[2] *Availability of Benchmarking option depends on a minimum number of considered subscribers to guarantee customer anonymity and data protection.*

SIEMENS Healthineers

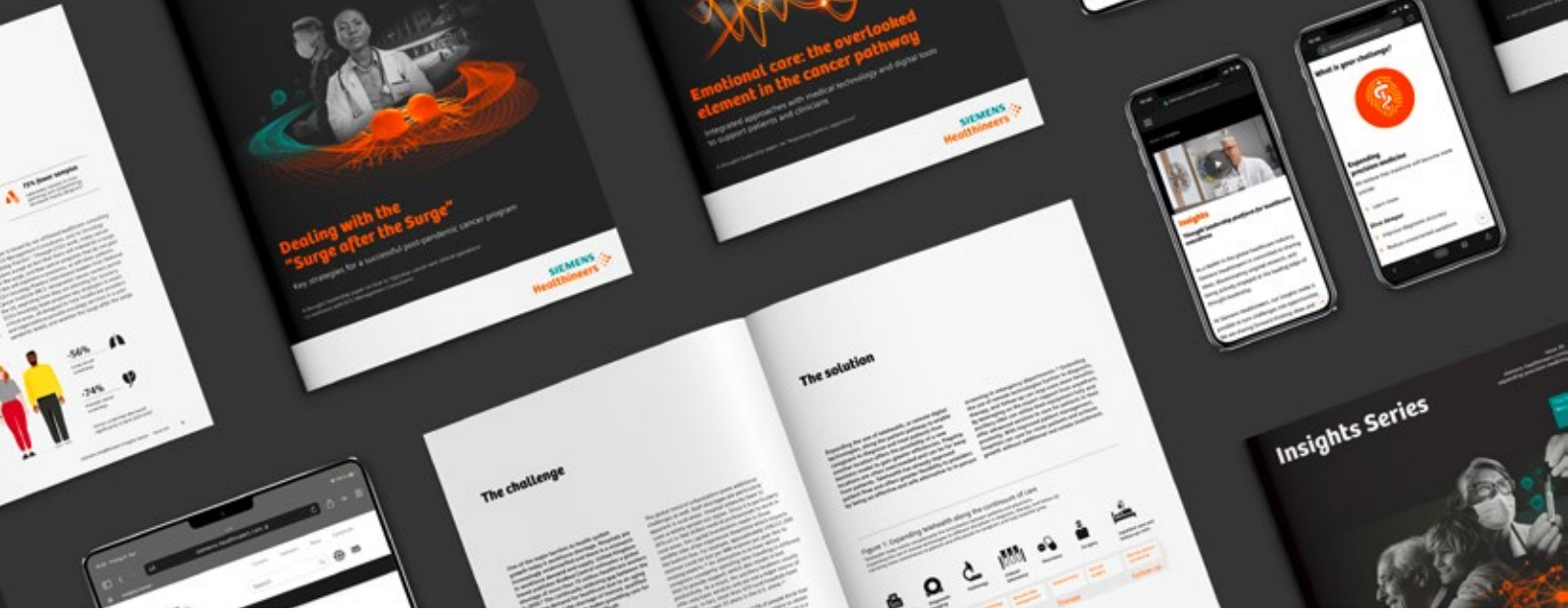

Insights Series

Ready for a new perspective?

Our preeminent thought leadership platform

The Insights Series – Selected Papers

All available at: siemens-healthineers.com/insights-series

Expanding precision medicine

The case for robotic-assisted PCI

What is the value for healthcare executives?

This paper examines various challenges associated with manual PCI, and then explores a potential solution—a rapidly emerging alternative to the complex, demanding procedure so many patients rely on today. The deployment of R-PCI offers an advance in precision, safety, and value that healthcare providers and organizations would do well to consider, and patients are likely soon to demand.

Expanding precision medicine

COVID-19 testing in the vaccine era

Challenges and solutions for healthcare executives

This paper looks into COVID-19 testing, which will continue to have a substantial impact on every aspect of hospital operation throughout the current vaccination era and for the foreseeable future. The paper addresses: quality of care, financial performance, personnel, organizational reputation, and COVID-19 protocols.

Transforming care delivery

Unlocking the digital front door

How healthcare can be made more accessible

This paper looks at the rise of digital access points to healthcare, at how provider-patient interactions can be done digitally, and identifies five main areas which help to unlock digital front doors to healthcare.

Improving patient experience

Emotional care: the overlooked element in the cancer pathway

Integrated approaches with medical technology and digital tools to support patients and clinicians

This paper is authored in cooperation with Sir Muir Gray, a recognized authority in public health and cancer care, and Nick Rowley, from iWantGreatCare. It proposes an easily applicable approach to early detection of stress, anxiety, and emotional distress along the entire oncology care pathway.

Improving patient experience & Digitalizing healthcare

Frictionless healthcare

Why it matters, how to get there?

This paper, written in collaboration with ECG Management Consultants, explores points of friction for both patients and healthcare providers, and proposes concrete steps and digital tools that can help this. In doing so, it lays out a roadmap for frictionless healthcare.

Subscribe

Subscribe to receive upcoming Insights Series papers directly to your e-mail inbox, containing thought-provoking ideas for the success of your healthcare institution.

The Insights Series can be found at: *siemens-healthineers.com/insights-series*

On account of certain regional limitations of sales rights and service availability, we cannot guarantee that all products included in this brochure are available through the Siemens sales organization worldwide. Availability and packaging may vary by country and is subject to change without prior notice. Some/All of the features and products described herein may not be available in the United States.

The information in this document contains general technical descriptions of specifications and options as well as standard and optional features which do not always have to be present in individual cases, and which may not be commercially available in all countries.

Due to regulatory reasons their future availability cannot be guaranteed. Please contact your local Siemens organization for further details.

Siemens reserves the right to modify the design, packaging, specifications, and options described herein without prior notice. Please contact your local Siemens sales representative for the most current information.

Note: Any technical data contained in this document may vary within defined tolerances. Original images always lose a certain amount of detail when reproduced.

Siemens Healthineers Headquarters
Siemens Healthcare GmbH
Henkestr. 127
91052 Erlangen, Germany
Phone: +49 9131 84-0
siemens-healthineers.com

Published by Siemens Healthcare GmbH · Order No. A91MR-1000-139C-7600 · Printed in Germany · 12464 0722 · ©Siemens Healthcare GmbH, 2022

siemens-healthineers.com/magnetom-world